THE QUARZ-CRYSTAL MICROBALANCE IN LIFE SCIENCE

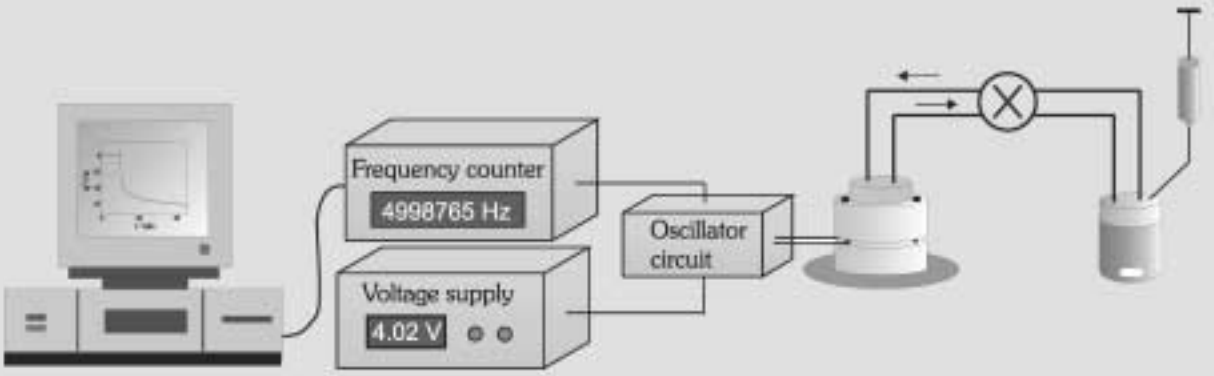

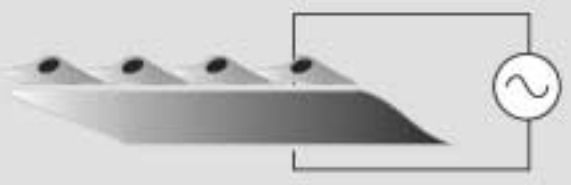

ANGEWANDTE CHEMIE

Piezoelectric Mass-Sensing Devices as Biosensors—An Alternative to Optical Biosensors?

Andreas Janshoff, Hans-Joachim Galla, and Claudia Steinem*

Dedicated to Professor Erich Sackmann on the occassion of his 65th birthday

In the early days of electronic communication—as a result of the limited number of quartz resonators available—frequency adjustment was accomplished by a pencil mark depositing a foreign mass layer on the crystal. In 1959, Sauerbrey showed that the shift in resonance frequency of thickness-shear-mode resonators is proportional to the deposited mass. This was the starting point for the development of a new generation of piezoelectric mass-sensitive devices. However, it was the development of new powerful oscillator circuits that were capable of operating thickness shear mode resonators in fluids that enabled this technique to be introduced into bioanalytic applications. In the last decade adsorption of biomolecules on functionalized surfaces turned in to one of the paramount applications of piezoelectric transducers. These applications include the study of the interaction of DNA and RNA with complementary strands, specific recognition of protein ligands by immobilized receptors, the detection of virus capsids, bacteria, mammalian cells, and last but not least the development of complete immunosensors. Piezoelectric transducers allow a label-free detection of molecules; they are more than mere mass sensors since the sensor response is also influenced by interfacial phenomena, viscoelastic properties of the adhered biomaterial, surface charges of adsorbed molecules, and surface roughness. These new insights have recently been used to investigate the adhesion of cells, liposomes, and proteins onto surfaces, thus allowing the determination of the morphological changes of cells as a response to pharmacological substances and changes in the water content of biopolymers without employing labor-intense techniques. However, the future will show whether the quartz-crystal microbalance will assert itself against established label-free sensor devices such as surface plasmon resonance spectroscopy and interferometry.

Keywords: analytical methods · biosensors · molecular recognition · quartz-crystal microbalance · surface chemistry

1. Introduction

As a consequence of their extraordinary properties quartz resonators can be found in all kinds of electronic devices, such as watches and computers to give an accurate time base, and as signal generators or reference systems in electronic devices. Quartz resonators did not become of interest commercially until immediately prior to World War II when there was an enormous requirement for communication devices. More than 30 million resonators were necessary to cover the demand. Quartz crystals attained significance as an analytical device after the discovery that there is linear relationship between deposited mass and the frequency response,[1, 2] as demonstrated by Sauerbrey in 1959.[3] He showed that this proportionality only holds if the ideal layer of foreign mass is strongly coupled to the resonator. This is the reason for calling such a device a "quartz-crystal microbalance" (QCM). The mass sensitivity of a 5 MHz quartz crystal is approximately 0.057 $Hz\,cm^2\,ng^{-1}$, which is approximately 100 times higher than that of an electronic fine-balance with a sensitivity of 0.1 μg. In the 1960s and 1970s the QCM technique gained importance as devices for monitoring thicknesses in vacuum and air, and is still used in today's laboratories to determine the thicknesses of layers. The lack of suitable oscillator circuits that enabled the shear-wave resonator to be operated in fluids prevented, however, the extension of this technique to bioanalytical areas. In 1982, Nomura and Okuhara[4] were the first to report on a circuitry capable of breaking this barrier, thus giving the starting point for the development of a new class of bioanalytic tools.

[*] Dr. C. Steinem, Dr. A. Janshoff, Prof. Dr. H.-J. Galla
Institut für Biochemie
Westfälische Wilhelms-Universität
Wilhelm-Klemm-Strasse 2, 48149 Münster (Germany)
Fax: (+49) 251-83-33-206
E-mail: steinec@uni-muenster.de

  1433-7851/00/3922-4005 $ 17.50+.50/0

Nowadays quartz resonators can be regarded as typical mechanical transducers for chemical and biological sensor devices that transform the mass or thickness of a foreign layer (physical quantity) of an analyte into an electrical signal. A mass adsorbed on a shear-wave resonator experiences an acceleration of more than 10^6 *g*. The amplitude of vibration is usually 10 – 20 nm in air and is reduced in water to a mere 1 – 2 nm.[5]

This article is intended to show that specific interactions between biomolecules can be quantified in terms of thermodynamic and kinetic parameters by means of QCM. Furthermore, the objective is to put emphasis on the fact that the QCM is more than just a mass sensor. A new application of this classical technique is the determination of viscoelastic properties of cellular systems. The strength of piezoelectric transducers is that they can couple mechanical and electrical variables, which allows the formulation of equivalent circuits that describe the mechanical properties of biopolymers and complex multilayers, such as confluent cell monolayers. Thus, it is possible to determine molecular recognition events apart from interfacial phenomena, surface energy, viscoelasticity, roughness, surface charge density, and the water content of biomolecules.

2. Basic Piezoelectric Resonators

2.1. Acoustic Waves in Solids

Acoustic waves cover a frequency range of 14 orders of magnitude—from 10^{-2} Hz (seismic waves) and extending to 10^{12} Hz (thermoelastic excited phonons; Figure 1). The acoustic resonators such as those mentioned in this article oscillate in a narrow frequency range of $10^6 – 10^9$ Hz.

A brief introduction to acoustic wave theory and in particular piezoelectric excited vibrations is given and then

A. Janshoff

H.-J. Galla

C. Steinem

Andreas Janshoff was born in 1966. He attended the Westfälische Wilhelms-University (WWU) Münster, where he received a B.S. in biology and chemistry. He received his M.S. in 1994 and his Ph.D. in 1997 for studies on the biofunctionalization of gold surfaces and its applications in bioanalytics, which he carried out at the Institute for Biochemistry at the university of Münster. As a postdoctoral fellow, he attended the group of M. Reza Ghadiri at the Scripps Research Institute, La Jolla (CA), USA for 18 months. During this time he worked on the imaging of lipid membranes by scanning force microscopy. In 1999 he returned to Germany, joining the group of Harald Fuchs at the WWU Münster to start his habilitation in close collaboration with the Institute for Biochemistry (WWU). His research fields include the development of new sensor systems based on micropatterned surfaces and the application of acoustic resonators as a tool to investigate biological relevant questions.

Hans-Joachim Galla, born in 1948, attended the university of Göttingen. After receiving his B.S. in chemistry in 1973, he received his Ph.D. in 1975 in Göttingen under the tutelage of Erich Sackmann for work on phase-separation phenomena and lipid – protein interactions carried out at the Max-Planck Institute for Biophysical Chemistry. In 1976 he changed to the Department of Biophysics at the university of Ulm as a research associate, where he finished his habilitation in 1979. At the same time (1979/1980) he was a research associate at Stanford university before he returned to the university of Ulm as a Heisenberg fellow. In 1983 he became professor of biophysical chemistry at the Institute for Biochemistry of the technical university of Darmstadt. In 1990 he took a professorship of biochemistry at the university of Münster. His main research fields include the differentiation of cerebral endothelia of the blood – brain barrier, monomolecular lipid – peptide layers as model systems for the alveolar lung surfactant, and biofunctionalization of solid-supported lipid membranes for applications in bioanalytics.

Claudia Steinem, born in 1967, attended the Westfälische Wilhelms-University in Münster, where she received a B.S. in biology and chemistry and a M.S. in chemistry. In 1997 she received her Ph.D. under the tutelage of Hans-Joachim Galla on studying the ion transport in solid-supported lipid bilayers. After a postdoctoral stay at the Scripps Research Institute in La Jolla, CA (USA) for 18 months in the group of M. Reza Ghadiri she returned as Lise-Meitner fellow at the Institute for Biochemistry of the Westfälische Wilhelms-University in 1999. She is currently organizing her own research group in the course of her habilitation. Her main research interests include the study of the interaction of artificial peptides, annexins, and proteins of the signal transduction pathway with lipids, and the development of new lipid membrane systems based on porous surfaces.

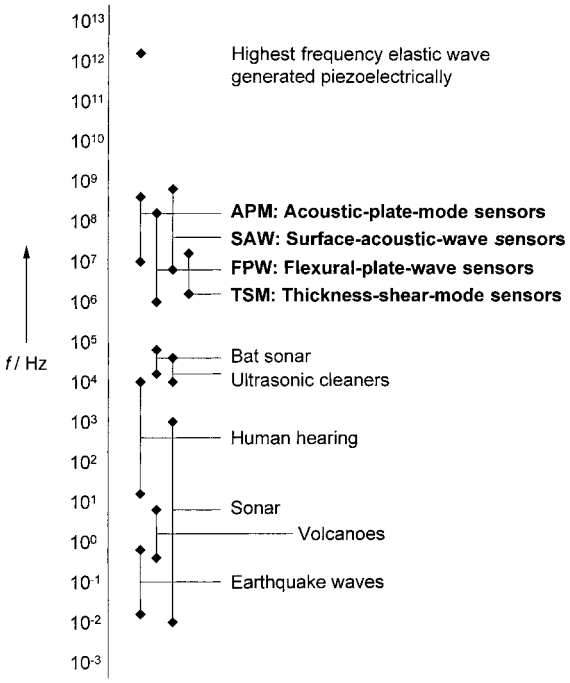

Figure 1. The spectrum of acoustic waves covers roughly 14 orders of magnitude. The frequency range of the four resonators which are described in this article range in operation between 1 and 1000 MHz.[7]

this is followed by a more detailed description of different types of piezoelectric transducers.

The application of a periodic perturbation (stress) to a solid results in elastic deformations (strain), which travel as waves through the solid. The type of wave—transversal or longitudinal—and the phase velocity both depend on the crystal structure. The wave equation that describes acoustic waves in solids [Eq. (1)] can be derived using the equation of motion, the definition of strain, and the constitutive equations.[6]

$$\nabla \cdot \boldsymbol{c} : \nabla_s \boldsymbol{u} = \rho \frac{\partial^2 u}{\partial t^2} \quad (1)$$

$\boldsymbol{u}$ is the displacement of the particle, ρ the density of the material, and t denotes time. The matrix $\boldsymbol{c}$ describes the elasticity moduli of the solid. Table 1 summarizes the relevant expressions for one and three dimensions.

Table 1. The dynamic equations of motion for one and three dimensions. **c** is the tensor of elasticity. Stress **T** and strain **S** are symmetric tensors with nine elements of which six are independent because of symmetry. u is the particle displacement, z indicates the direction where strain occurs, and ρ is the density of the material.[6]

	One-dimensional system	Three-dimensional system
Newton's law	$\frac{\partial T}{\partial z} = \rho \frac{\partial^2 u}{\partial t^2}$	$\nabla \cdot \mathbf{T} = \rho \frac{\partial^2 u}{\partial t^2}$
definition of stress	$S = \frac{\partial u}{\partial z}$	$\mathbf{S} = \nabla_s \boldsymbol{u}$
constitutive relations		
Hooks law	$T = CS$	$\boldsymbol{T} = \boldsymbol{c} : \boldsymbol{S}$
particle velocity	$v = \frac{\partial u}{\partial t}$	$v = \frac{\partial u}{\partial t}$
mechanical impedance	$Z = \sqrt{\rho C}$	
phase rate	$v_p = \sqrt{C/\rho}$	

2.2. Piezoelectric Excited Acoustic Waves in Solids

Piezoelectricity as first reported 1880 by the Curie brothers describes the generation of electrical charges on the surface of a solid caused by pulling, pressure, or torsion. In contrast, the occurrence of a mechanical deformation arising from an external electric field is called the converse piezoelectric effect. Figure 2 shows schematically the general relationships between mechanical and electrical variables.

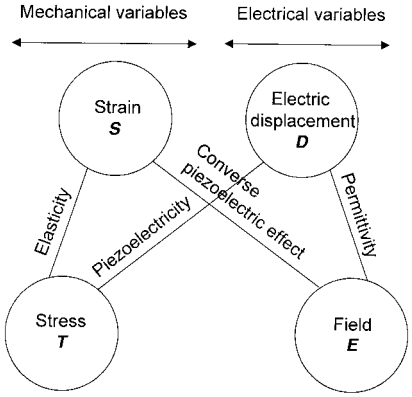

Figure 2. Relationship between mechanical and electrical variables. The direct piezoelectric effect is the production of electric displacement by applying a mechanical stress. The converse piezoelectric effect results in a strain in the crystal when an electrical field is applied. The relation between stress and strain is determined by the elasticity of the solid.[7]

Prerequisite for the occurrence of piezoelectricity in crystals is an inversion center. In total 21 point groups fulfill this requirement but only 20 classes have nonzero piezoelectric constants. Although a large number of crystals show piezoelectricity only quartz provides the unique combination of mechanical, electrical, chemical, and thermal properties, which has led to its commercial significance. Equation 1 needs to be expanded by the term $\boldsymbol{e}\nabla^2\Phi$ in order to introduce piezoelectricity in the general wave equation, in which Φ is the electrical potential and $\boldsymbol{e}$ the piezomodul composed of piezoelectric constants as matrix elements.[7] The additional expression is responsible for the electrical excitation of elastic waves in a piezoelectric solid. The resulting motion causes a change in Φ, which can in turn be detected electrically. Since the gradient of the displacement current is zero, that is, no free charge density occurs, integration of the extended Equation (1) results in a comprehensive expression that describes acoustic waves in a piezoelectric medium. The following section deals with its physical consequences.

2.3. Piezoelectric Resonators

The main emphasis of this article is placed on bulk-acoustic-wave (BAW) or thickness-shear-mode (TSM) resonators, which are also known as quartz-crystal microbalances (QCMs). Although TSM resonators are considerably less sensitive than flexural-plate-wave (FPW) or surface-acoustic-wave (SAW) sensors they are widely used as a result of their robust nature, availability, and affordable electronics. Figure 3 depicts schematically various resonator types.

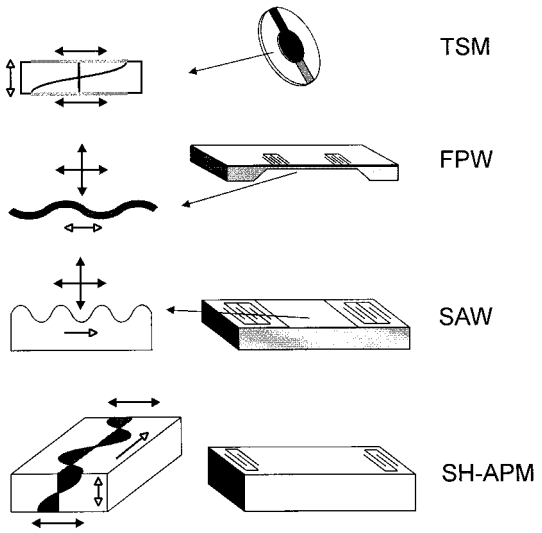

Figure 3. Schematic sketches of the four common types of acoustic resonators and their wave propagation modes. The particle displacement is indicated by a black arrow, and the direction of the wave propagation by an open arrow. TSM: thickness-shear-mode resonator, also known as the quartz-crystal microbalance technique; FPW: flexural-plate-wave resonator; SAW: surface-acoustic-wave resonator (two port delay line) and SH-APM: shear-horizontal-acoustic-plate-mode resonator.

2.3.1. Thickness-Shear-Mode (TSM) Resonators (Quartz-Crystal Microbalances)

Depending on the cut-angle a large number of different resonator types such as thickness-shear-mode, plate, and flexural resonators can be obtained from a mother crystal (Figure 4A) with eigenfrequencies ranging from $5 \times 10^2 - 3 \times 10^8$ Hz. Generally, AT-cut crystals are used for QCM purposes, being cut with an angle of 35.25° to the z-axis (Figure 4B). AT-cut quartz crystals exhibit a high frequency stability of $\Delta f/f \approx 10^{-8}$, which makes them well-suited for many electronic devices.[8, 9]

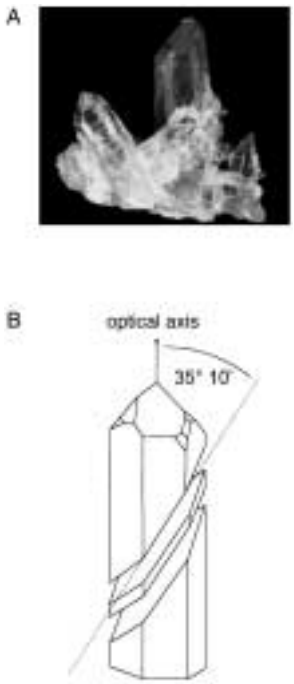

Figure 4. A) Photograph of several α-quartz crystals. B) AT-cut of a quartz crystal. A quartz plate is cut at an angle of 35° 10′ with respect to the optical axis. A deviation of only 5′ from the angle leads to a temperature coefficient that is different from zero in the range of 0–50 °C.

Since AT-cut quartz crystals have a temperature coefficient that is almost zero between 0–50 °C, this particular cut is the most suitable one for QCM sensors.[10] The following parameters are always related to AT-cut quartz.

A convenient way to describe acoustic waves traveling in a circular, lossless, and stress-free AT-cut crystal with thickness d_q is to express the wave equation in cylindrical coordinates (Figure 5). The propagation velocity of the acoustic wave in a piezoelectric thickness-shear-mode resonator is $(\bar{c}_{66}/\rho_q)^{1/2}$ (ρ_q = density of the quartz).[11] The boundary conditions require that the amplitude of the shear displacement is zero at the electrode edges, while it is at a maximum at $r = 0$ and exhibits a node at $z = 0$. θ follows periodic boundary conditions. The wave equation can be solved by a usual separation process.[12] The solution yields important properties of the shear vibration. The eigenfrequencies are found in general from Equation (2).[9]

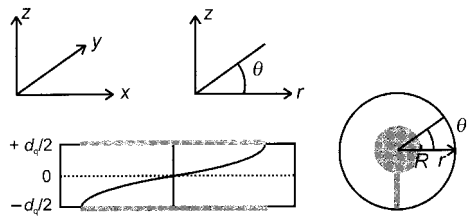

Figure 5. Definition of the coordinates of a circular-shaped quartz crystal. The gray areas depict the metal electrodes.

$$f_{mnk} = \frac{v_p}{2\pi}\sqrt{\frac{n^2\pi^2}{d_q^2} + \frac{\lambda_{mk}^2}{R^2}} \overset{R \gg d_q}{\approx} \frac{v_p}{2\pi}\sqrt{\frac{n^2\pi^2}{d_q^2}} = \frac{v_p n}{2\,d_q} = \frac{nK_R}{d_q} \qquad (2)$$

From the solution of the wave equation, it is clear that only odd overtones n can be excited.[13] The displacement at $r = 0$ and $z = \pm d_q/2$ is at a maximum for the fundamental frequency, while the amplitude vanishes at the electrode edges where $r = R$. Thus, the transversal wave exhibits a node at $z = 0$ and maximum amplitude at $z = \pm d_q/2$.[14]

If the lateral dimensions of the quartz plate greatly exceeds the thickness of the crystal the problem can be treated one-dimensionally. The function $u_x(z,t)$ describes two transversal waves traveling in opposite directions, which thus form a standing wave within the crystal. Assuming stress-free surfaces ($\partial u/\partial z = 0$), the shear vibration can be described as a simple cosine function. The use of constructive interference $d_q = n\lambda/2$ and $R \gg d_q$ simplifies Equation (2).[15] K_R denotes the so-called frequency constant of AT-cut quartz with $K_R = 1664\ \mathrm{m\,s^{-1}}$.[9] It can be deduced from Equation (2) that the resonance frequency of an AT-cut quartz increases with decreasing thickness of the crystal. For instance, a 5 MHz quartz exhibits a thickness of 0.33 mm, while a 30 MHz crystal is only 55 μm thick.

TSM resonators provide numerous material-specific parameters. In order to fully exploit the capability of acoustic resonators it is essential to understand the conversion between mechanical and electrical parameters since the last ones are those which are readily accessible to the user. Mechanical models can readily be transformed into equivalent electrical circuits which permit a complete description of the oscillation in the presence of an adsorbent. A general one-dimensional acoustic wideband model has been suggested by Mason[16] (Figure 6A) and provides a basis for the theoretical description of complex composite resonators as they occur in life science. In particular cases, such as low load, the Mason model can be easily transformed near resonance into an equivalent circuit with lumped elements—the so termed Butterworth–van-Dyke (BVD) circuit (Figure 6B). A comprehensive treatment of this issue has been given by Rosenbaum.[6]

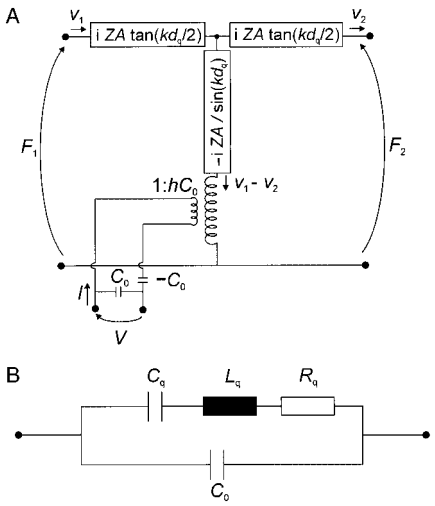

Figure 6. A) Equivalent circuit (wideband model) of the three-port Mason model of a finite thickness piezoelectric layer. The equivalent circuit consists of two mechanical ports and one electrical port. Z is the characteristic impedance of the quartz, k the complex wave number, A the area, and d_q the thickness of the resonator. hC_0 is the turns ratio of the transformer and is defined as $(e_{26}/\varepsilon_{22})C_0$. B) Butterworth–van-Dyke-equivalent circuit. Near resonance the three-port Mason model can be transformed into an equivalent circuit composed of discrete impedance elements. The capacitance C_q represents the mechanical elasticity of the quartz, the inductance L_q the initial mass, and the resistance R_q the energy losses arising from viscous effects, internal friction, and damping induced by the crystal holder. The static capacitance C_0 determines the admittance away from resonance, while the motional components dominate near resonance.[6]

Table 2. Parameters of the BVD-equivalent circuit and their relationship to the physical characteristic numbers of an AT-cut quartz together with the different resonance frequencies. A is the electrode area, η_q the viscosity, d_q the thickness of the quartz, ε_{22} the dielectric constant of the quartz material, and e_{26} the piezoelectric constant dependent on the cutting angle, which can be obtained from the matrix elements e_{11} and e_{14} of the piezoelectric polarization modulus $\boldsymbol{e}$ and the cutting angle. The material constants shown in this Table are only valid for AT-cut quartz.[9]

Parameter	Expression
C_0	$\dfrac{\varepsilon_{22}A}{d_q}$
C_q	$\dfrac{8Ae_{26}^2}{\pi^2 d_q \bar{c}_{66}}$
L_q	$\dfrac{d_q^3 \rho_q}{8Ae_{26}^2}$
R_q	$\dfrac{d_q \eta_q \pi^2}{8Ae_{26}^2}$
f_s	$\dfrac{1}{2\pi}\sqrt{\dfrac{1}{L_qC_q}}\left(1+\dfrac{C_0R_q^2}{2L_q}\right)$
f_p	$\dfrac{1}{2\pi}\sqrt{\dfrac{1}{L_qC_q}}\left(1+\dfrac{C_q}{2C_0}-\dfrac{C_0R_q^2}{2L_q}\right)$
f_{Zmin}	$\dfrac{1}{2\pi}\sqrt{\dfrac{1}{L_qC_q}}\left(1-\dfrac{C_0R_q^2}{2L_q}\right)$
f_{Zmax}	$\dfrac{1}{2\pi}\sqrt{\dfrac{1}{L_qC_q}}\left(1+\dfrac{C_q}{2C_0}+\dfrac{C_0R_q^2}{2L_q}\right)$

The BVD circuit combines a parallel and series resonance circuit (motional branch). The motional branch consists of L_q, C_q, and R_q. The electrodes on both sides of the crystal plate provide an additional parallel capacitance C_0, which gives rise to a parallel circuit. Table 2 summarizes the expressions for L_q, C_q, R_q, and C_0 as they occur at the fundamental vibration.

The quartz material between the two electrodes (Figure 5) serves as a typical dielectric material, thus the resonator behaves as a plate condenser at high frequencies. Figure 7 displays parameter curves of impedance spectra of a 5 MHz quartz crystal on varying L_q, C_q, R_q, and C_0. The motional resistance R_q contains intrinsic viscosities of the quartz and is responsible for energy dissipation. The phase maximum is a measure of the damping of a quartz resonator, as pointed out by Martin et al.[17]

If damping is negligible ($R_q \rightarrow 0$) the quartz resonator shows two resonance frequencies corresponding to a phase shift $\varphi = 0$ at minimum and maximum magnitudes of the impedance $|Z|$. The corresponding resonant frequencies are referred to as resonant frequency f_R and antiresonant frequency f_A.[9, 18, 19] The separation between the frequencies rises with an increase in the electroacoustic coupling constant K. Four different resonant frequencies

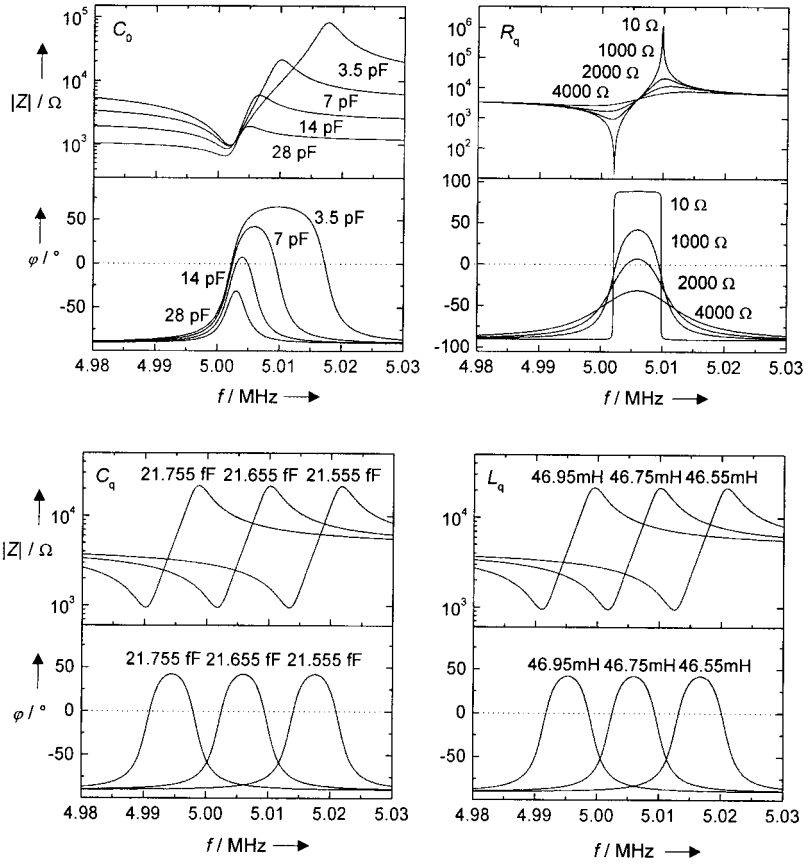

Figure 7. Simulated impedance spectra from the BVD-equivalent circuit with discrete variations of the impedance element values C_0, C_q, L_q, and R_q.

are discernable if damping occurs ($R_q > 0$; Figure 8A). f_R separates into f_{Zmin}, the frequency at minimal impedance ($|Z|$), and f_s, the frequency at zero phase φ at the low frequency branch. In turn f_A separates into f_p, the frequency at zero phase at the high frequency branch, and f_{Zmax}, the frequency at maximum impedance. The expressions for f_s, f_p, f_{Zmin}, and f_{Zmax} assuming low R_q and their dependencies on the electrical parameters of the simple BVD equivalent circuit are given in Table 2.

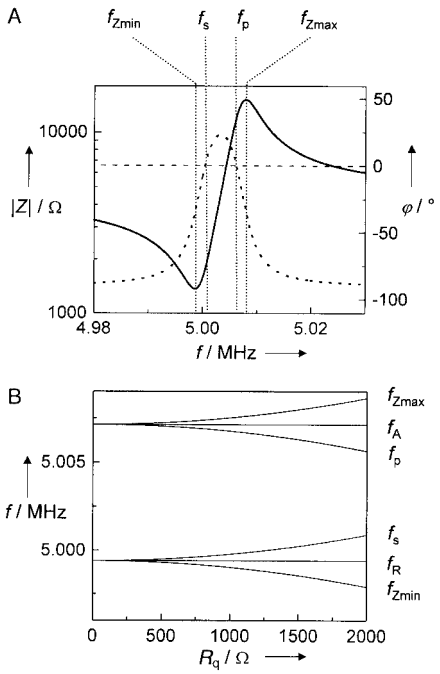

Figure 8. A) Simulated impedance spectrum from the BVD-equivalent circuit with marked resonance frequencies f_{Zmin}, f_s, f_p, and f_{Zmax} for the case of $R_q > 0$. B) Dependence of the resonance frequencies f_{Zmin}, f_s, f_p, and f_{Zmax} on the motional resistance R_q calculated according to the approximation of Bottom.[9] Accurate calculations show that f_s and f_p converge at $R_q =$ 2280 Ω.

The dependence of the resonance frequency on the damping resistance R_q are shown in Figure 8B. f_{Zmax} and f_s rise with increasing damping, while f_{Zmin} and f_p decrease. The resonant frequencies f_s and f_p converge at $\varphi_{max} = 0$.

Active oscillation of shear resonators is restricted to $\varphi_{max} > 0$. At larger resistances leading to $\varphi_{max} \leq 0$ impedance analysis by a network analyzer is necessary to further study the behavior of the resonator.

2.3.1.1. Mass Loading

Sauerbrey has provided the first treatment of this issue.[3] By analytically solving the one-dimensional equation of motion he showed that an ideal layer of foreign mass results in a frequency decrease Δf that is proportional to the deposited mass Δm if the resonator is operated in air or vacuum. If the density of the mass layer is equal to that of the quartz crystal, Equation (3) applies.

$$\Delta f = -\frac{2 f_0^2}{A \sqrt{\bar{c}_{66} \rho_q}} \Delta m = -S_f \Delta m \qquad (3)$$

Equation (3) describes the frequency response of a resonator on deposition of thin, rigid, and uniform films. The integral mass sensitivity or Sauerbrey constant S_f depends on the square of the fundamental frequency [Eq. (3)], and increases proportionally to the overtone number.

The differential mass sensitivity, however, is maximum in the center of the quartz resonator and decreases towards the borders of the electrodes (Figure 9).

The concept of energy trapping explains the differential mass sensitivity observed.[6] The conditions for resonance and hence the resonant frequencies of the quartz crystal in the electrode-free region are different from those at the electrodes as a result of the additional mass of the electrodes. Analogous to the total reflection of light in an optical waveguide, in which the incoming light cannot penetrate the optically more dense material, standing acoustic waves generated at the electrodes are confined to this region, and is referred to as energy trapping. The lateral components of the acoustic wave, which travel tangential to the surface of the crystal are almost completely reflected at the interface between the electrode and electrode-free region. Energy trapping suppresses spurious modes and the quality factor of the resonator increases.[20] However, if the thickness of the electrodes is too thin (usually less than 500 Å) the resonant frequencies of regions with and without electrodes are very similar, so that the acoustic wave is not confined to the electrode-covered region, and as a consequence the quality factor Q of the resonator decreases. Very thick electrodes, however, cause a decrease in the Q-factor as a result of the

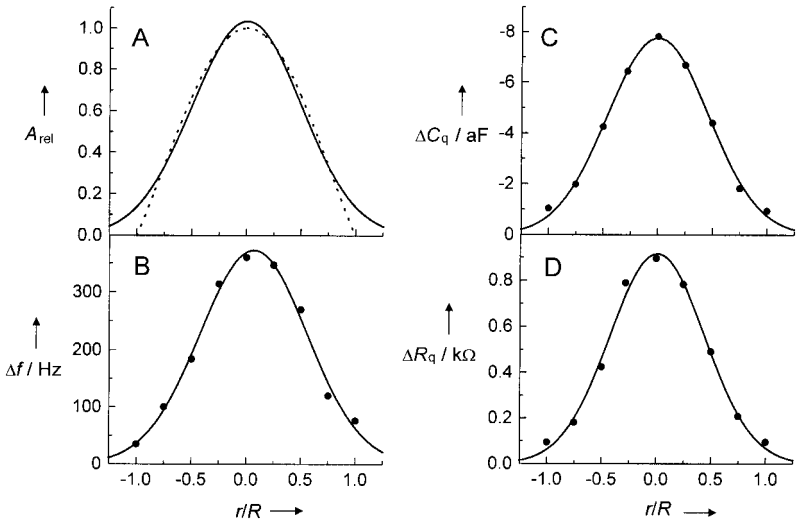

Figure 9. A) Radial distribution of the relative oscillation amplitude at the quartz surface according to a Bessel distribution (dotted line) and a Gaussian distribution (solid line) with $a = 2$. The Bessel function drops to zero at the electrode edges where $r/R = 1$, whereas the Gaussian function includes motion near the electrode edges. B) The increase in frequency of a 5 MHz AT-cut quartz while pressing a polyethylene tip on the quartz surface immersed in water. The change in resonance frequency is defined as $\Delta f = f(r) - f_o$. C) Corresponding capacitance change c_q of a 5 MHz AT-cut quartz. D) Change in motional resistance R_q. The solid lines are the results of the fitting parameters of a Gaussian distribution to the data.

presence of a dead dielectric, which is particularly pronounced by using gold electrodes and high frequency resonators.[21] Electrodes made of aluminum instead of gold improve the situation because of the lower acoustic adsorption coefficient of aluminum. Further improvement can be achieved by using larger electrode areas.

The radial mass sensitivity s_f is proportional to the square of the radial displacement ($s_f(r) \propto |u(r)|^2$),[22] which is described by a Bessel function J_0 of the first kind and zeroth order (Figure 9A).[12] The highest sensitivity is located at the center of the crystal at $r = 0$ and vanishes at the electrode edges. However, Martin and Hager[23] were the first to show that the amplitude of vibration is nonzero beyond the electrode edges ($r = R$) as a result of field fringing (inhomogeneous electric field, Figure 16), which is not considered by the energy-trapping concept. Field fringing is enhanced in an environment of higher permittivity such as water. The amplitude of the shear vibration depends on energy dissipation and therefore on the kind of load on the quartz. Liquid loading usually results in considerable damping and increased field fringing leading to a broadening of the curve and a decreased amplitude. The radial distribution of the shear amplitude can empirically be described by a Gaussian function [Eq. (4)].[23]

$$u(r) = u_{max} \exp\left(-a\frac{r^2}{R^2}\right) \quad (4)$$

u_{max} denotes the maximum displacement at $r = 0$ and a is the characteristic width of the distribution, with typical values of $a \approx 2$ for a plane–parallel 5 MHz quartz in water. Figure 9A displays a comparison of the two distributions. The spatial distribution of the differential mass sensitivity can be experimentally probed by depositing small defined masses or attaching a sharp probe at certain locations of the crystal surface. The latter approach has been used to map the sensitivity distribution of a 5 MHz quartz resonator as shown in Figure 9B–D. The maximum change of Δf, ΔR_q, and ΔC_q occurs in the center of the plate. The distribution is well described by an empiric Gaussian function. By including field fringing, Hillier and Ward[12] provided a solution of the wave equation that shows proportionality between frequency shift and deposited mass only if the material is homogeneously distributed over the crystal. Employing electrolysis to calibrate the QCM, however, does not always result in the formation of homogeneous metal films but often leads to an increased amount of deposited material at the electrode edges, which thus results in a systematic underestimation of the integral mass sensitivity.

The Sauerbrey Equation does not apply for thick films, viscous liquids, elastic solids, and viscoelastic bodies. In order to describe these various types of loading, theoretical models are needed to account for the observed frequency shifts and impedance spectra.[24–29] Furthermore, the development of special oscillator circuits was necessary to cope with the high damping with liquid loads. Since the theoretical description of composite loading is common in life science problems and biosensor applications are of paramount interest, the theoretical framework developed by Bandey et al.[25] has been chosen in this Review to explain some of the most relevant load situations in bioanalytics.

Starting with the three-port-Mason model (Figure 6A) the piezoelectric resonator loaded on one side can be characterized by its mechanical impedance Z_s [Eq. 5] (T_{xz} = mechanical strain in the xz direction; V_x = potential in the x direction).

$$Z_s = \left.\frac{T_{xz}}{V_x}\right|_{z=0} \quad (5)$$

The electrical impedance of the system Z_m is composed of Z_m^0 [Eq. (6a)], the impedance of the unperturbed resonator, and a term Z_m^1 [Eq. (6b)] representing the load (ω = angle frequency).

$$Z_m^0 = \frac{1}{i\omega C_0}\left(\frac{k\,d_q/K^2}{2\tan(kd_q/2)} - 1\right) \approx R_q + i\omega L_q + \frac{1}{i\omega C_q} \quad (6a)$$

$$Z_m^1 = \frac{k\,d_q(Z_s/Z_q)}{4K^2\omega C_0}\left(1 - \frac{i(Z_s/Z_q)}{2\tan(kd_q/2)}\right)^{-1} \approx \frac{n\pi}{4K^2\omega_s C_0}\frac{Z_s}{Z_q} \quad (6b)$$

K is the electroacoustic coupling factor. The approximations on the right hand side are only valid for low-load conditions of the quartz ($Z_s/Z_q < 2\tan(kd_q/2)$). If $Z_s/Z_q \leq 0.1$ the impedance of the loaded resonator can be expressed as a lumped element equivalent circuit with Z_m^1 (Figure 10) as an additional element in series to the motional branch of the BVD-equivalent circuit (Figure 6B). The mechanical impedance Z_s is a complex number in which the real part represents mechanical energy losses whereas the imaginary part stands for mechanical energy storage at the surface. Table 3 shows the impedance elements of Z_s for various surface coatings.

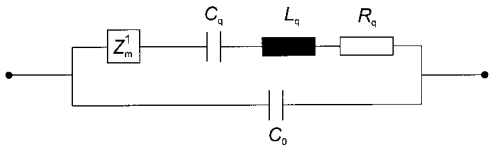

Figure 10. Modified BVD-equivalent circuit with an additional complex impedance Z_m^1 representing the load on the surface.

Table 3. Mathematical expressions of motional inductance L_L and resistance R_L for particular loads on AT-cut quartz resonators.[25]

Load	L_L	R_L
rigid mass	$\frac{n\pi}{4K^2\omega C_0}\frac{\rho_S}{Z_q}$	0
Newtonian liquid	$\frac{n\pi}{4K^2\omega C_0 Z_q}\sqrt{\frac{\rho_L\eta_L}{2\omega}}$	$\frac{n\pi}{4K^2\omega C_0 Z_q}\sqrt{\frac{\omega\rho_L\eta_L}{2}}$
semi-infinite viscoelastic layer	$\frac{n\pi}{4K^2\omega C_0 Z_q}\left[\frlac{\rho_V(\lvert G\rvert - G')}{2}\right]^{1/2}$	$\frac{n\pi}{4K^2\omega C_0 Z_q}\left[\frac{\rho_V(\lvert G\rvert + G')}{2}\right]^{1/2}$

Equations (6a) and (6b) enables one to describe typical load situations such as thin rigid films, viscous liquids, and viscoelastic polymers.[25, 30, 31] Multilayers consisting of different kinds of surface layers can be described as a linear combination if interaction terms occurring between the different materials can be neglected. Nonlinearities will be discussed in more detail later. Three relevant cases, which are particularly interesting for applications in life science, are

thoroughly discussed in the following section: a) thin rigid films covered by a Newtonian liquid, b) semi-infinite viscoelastic solids, c) thin viscoelastic solids covered by a Newtonian liquid.

2.3.1.1.1. With a Newtonian Liquid Covering Thin Rigid Films

Covering a sufficiently thin film[32] with a semi-infinite Newtonian liquid permits a linear combination of the mechanical impedances of the rigid mass and the liquid (Figure 11).

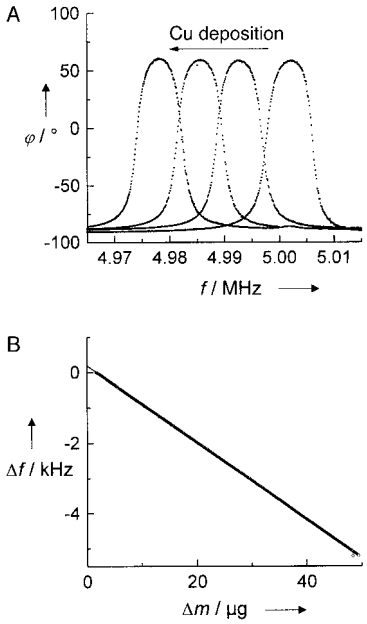

Figure 11. A) Impedance spectra of a 5 MHz AT-cut quartz before and after sequential deposition of 79, 158, and 237 µg of copper. The measurement was performed with one side of the quartz in contact with water. B) Change in the resonance frequency with increased amount of deposited copper.

The mechanical impedance of a rigid film of mass per unit area ρ_S can be expressed by $Z_s = i\omega\rho_s$. Z_s is purely imaginary, which means that the mass vibrates in phase with the resonator surface. The mechanical impedance Z_s of a liquid with viscosity η_L and density ρ_L can be determined from the velocity profile of a laminar flow parallel to the surface of the crystal [Eq. (7)], where $\delta = \sqrt{2\eta_L/(\omega\rho_L)}$ is the decay length of the damped shear wave within the fluid.

$$v_x(z,t) = v_{x,0}\, e^{-z/\delta} \cos(z/\delta)\, e^{i\omega t} \quad (7)$$

The shear wave propagates deeper into the medium with increasing kinematic viscosity (η_L/ρ_L). For instance, the decay length of a 5 MHz quartz is 250 nm in water. Assuming a mass load of a Newtonian liquid with a mass of $\Delta m = A\rho_L\delta$, Equation (3) results in the well-known expression found by Kanazawa and Gordon[29] [Eq. (8)], who related the product of the density and viscosity of the liquid to the frequency shift of the shear wave resonator.

$$\Delta f = -f_0^{3/2}\sqrt{\frac{\eta_L\rho_L}{\pi\rho_q\bar{c}_{66}}} \quad (8)$$

Kanazawa and Gordon did not consider the damping of the resonator from viscous loading. However, the electromechanical model of Martin and co-workers[17, 25] shows that the resistance R_L and the inductance L_L both exhibit a proportionality to the square root of the density-viscosity product of the corresponding liquid (Figure 12 A and B).

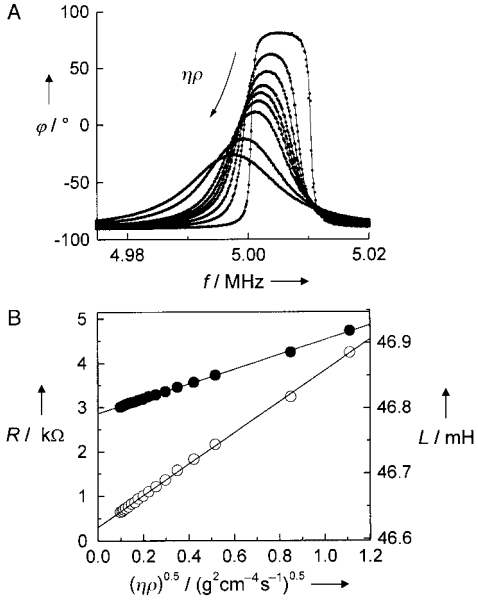

Figure 12. A) Influence of various glycerol–water mixtures on the phase shift. The solid lines are the results of fitting the parameters of the BVD-equivalent circuit. The measurements were taken in air (spectrum with the largest phase maximum), in water, as well as with glycerol–water mixtures of 40, 55, 60, 65, 70, 80, 85% glycerol (the arrow indicates an increasing amount of glycerol in solution).[167] B) Dependence of the resistance R (○) and inductance L (●) on the square root of the density/viscosity product of various glycerol–water mixtures. The parameters were fitted using the generalized BVD-equivalent circuit composed of L, C, R, and C_0. The capacitance C (21.655 fF) can be calculated from the intrinsic properties of the unloaded quartz (5 MHz).

A thin layer of a rigid mass covered by a semi-infinite layer of Newtonian liquid yields a linear combination, that is, addition of both impedances. The corresponding elements R_L and L_L can be obtained from a linear combination of the expressions shown in Table 3. Impedance spectra illustrating the situation of sequentially deposited copper films on a quartz crystal vibrating in aqueous solution are shown in Figure 11. Mass deposition of thin rigid films in a Newtonian liquid at constant density and viscosity can be described by Sauerbrey's equation without changes in R_L (Figure 11B).

2.3.1.1.2. Semi-Infinite Viscoelastic Solids

The semi-infinite viscoelastic solid is characterized by the absence of reflections at the air–solid interface of the shear wave traveling within the viscoelastic body. The decay length is smaller than the thickness of the solid. Therefore, wave propagation is unidirectional within the viscoelastic solid of density ρ_V, which leads to a simple expression for the mechanical impedance Z_s [Eq. (9)].[25]

$$Z_s = \sqrt{G\rho_v} \quad (9)$$

G is the complex shear modulus, in which Re(G) is the storage modulus G' and Im(G) the loss modulus G''. Both G'. and G'' can be obtained from the expression of R_L and L_L. Using a specific model for viscoelastic solids, such as the Kelvin or Voight model, one can calculate viscosity and elasticity, respectively. Figure 13 shows the frequency response and the shear displacement for different viscoelastic materials.

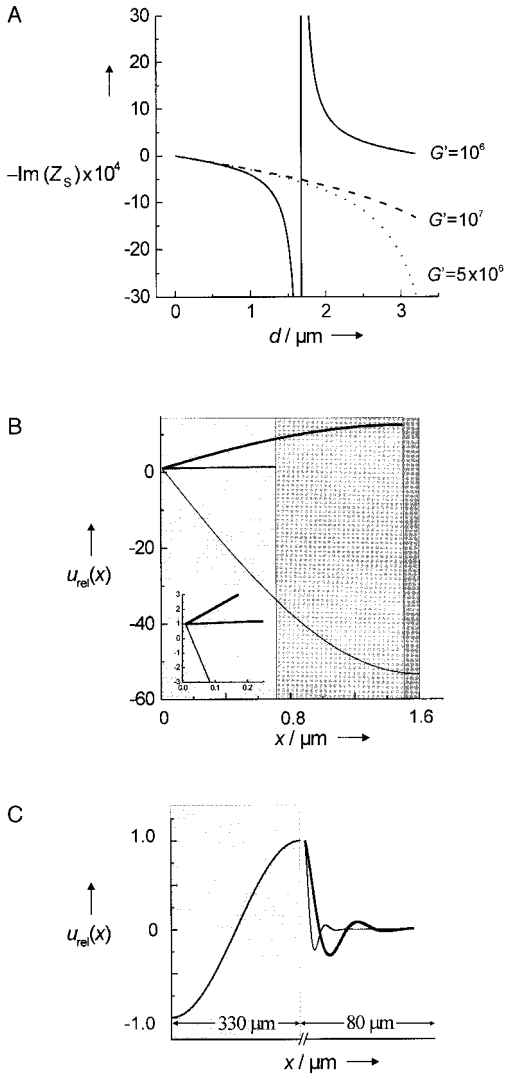

Figure 13. A) Numerical simulations of the imaginary part of the mechanical impedance (proportional to the frequency change) of a lossless viscoelastic film with different film thicknesses. An increase of film softness, namely, the shear modulus G becomes smaller, and leads to a considerable deviation from the Sauerbrey Equation even at small film thicknesses. For very soft films, even the resonance of the film is visible in the observed film thickness range, which starts at $\phi = \pi/2$ and is characterized by a sudden increase in the resonance frequency. B) Shear vibration amplitude within the film. Within the linear region of Im(Z_s) versus d the polymer surface oscillates in phase with the quartz and the damping is almost zero (middle curve). With larger thicknesses an overshoot of the displacement at the film/air interface occurs; the surface of the elastic film does move synchronously with the quartz oscillation but with a higher amplitude (top curve). Immediately after resonance the oscillation of the film is 90° behind the oscillation of the vibrating quartz (bottom curve). C) Within an infinite extended viscoelastic solid the shear oscillation propagates with different wave and decay lengths. The situation depends on the complex shear modulus G and the density of the solid.

2.3.1.1.3. With a Newtonian Liquid Covering Thin Viscoelastic Solids

The combination of a sufficiently thin viscoelastic film covered by a semi-infinite layer of a Newtonian liquid cannot be treated as a simple linear combination of the individual mechanical impedances as was valid for the two previous examples. Instead, interaction terms between the two different materials have to be taken into account. Granstaff and Martin[26] derived a general recursion formula [Eq. (10)] for a layer system with n different viscoelastic materials.

$$Z_s = Z_s^{(n)} \frac{Z_s^{(n+1)} \cosh(\gamma^{(n)} d^{(n)}) + Z_s^{(n)} \sinh(\gamma^{(n)} d^{(n)})}{Z_s^{(n)} \cosh(\gamma^{(n)} d^{(n)}) + Z_s^{(n+1)} \sinh(\gamma^{(n)} d^{(n)})} \quad (10)$$

γ denotes the complex wavenumber ik and $Z_s^{(n)}$ is the characteristic impedance of the nth viscoelastic layer. The procedure for evaluating the mechanical impedance of single layers is to start with the knowledge of the characteristic impedance of the top layer (stress free). Then, one has to work backward toward calculating the surface mechanical impedance at the resonator–film interface. This process allows the influence of many viscoelastic layers on the surface of the TSM resonator to be estimated, although extracting physical properties becomes cumbersome with increasing amount of layers. One example is a thin viscoelastic film of thickness d covered by a liquid. A description with discrete impedance elements is permitted because of the phase lag of the shear oscillation at the surface of the viscoelastic film with respect to the resonator–film interface. Resonance of the viscoelastic solid is reached at an acoustic phase shift $\phi = \omega d \,\mathrm{Re}\sqrt{\rho_v / G}$ of $\pi/2$ accompanied by a sudden increase in the resonance frequency and damping of the system (Figure 13). At $\phi > \pi/2$ the surface of the film oscillates at 90° to the surface of the resonator, and exhibits higher amplitude (overshoot) than the quartz material, which is almost critically damped.

2.3.1.1.4. Conclusion

The previous examples demonstrate that the operation of TSM resonators in liquids raises theoretical and experimental problems. Besides the difficult evaluation of multilayers composed of different viscoelastic solids or fluids, contributions from the electrolyte, roughness of the surfaces, surface energy of the outermost layer, and influence of compressional waves have to be considered. Some of the most important aspects are discussed in more detail below.

2.3.1.2. Longitudinal waves

Longitudinal or compressional waves can readily be observed by filling a measuring chamber equipped with a TSM resonator at the bottom and opened to air with a volatile liquid. Periodical changes in the resonant frequency can be recorded (Figure 14) as a result of the evaporation of the liquid. Closing the chamber, however, abolishes the observed instability instantaneously.

This observation can be explained in terms of compressional wave generation. The evaporation of the liquid with time results in the height of the liquid varying, and therefore constructive and destructive interference of the compres-

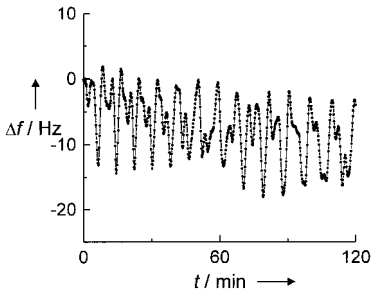

Figure 14. Periodic changes in the resonance frequency of a 5 MHz quartz immersed in ethanol. As ethanol evaporates over time, the resonance condition of the longitudinal wave, which is reflected at the ethanol – air interface, alters continuously.

sional waves reflected at the air – liquid interface occurs. This process results in a typical standing wave pattern. The origin of longitudinal waves can be reasoned by the occurrence of longitudinal or flexural modi or as shown by Martin and Hager[23] by a nonzero velocity gradient of the shear oscillation along the *x*-axis (Figure 15).

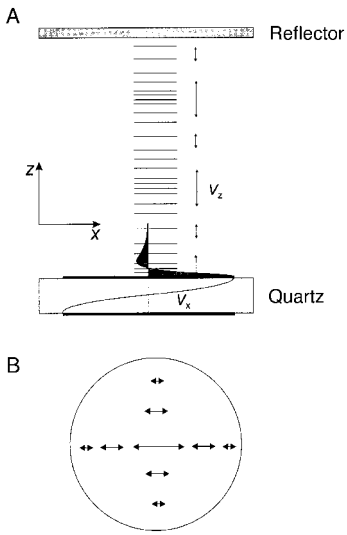

Figure 15. A) Representation of compressional waves generated in the fluid above the quartz crystal induced by a velocity gradient of the particle displacement, which are reflected at the glass surface and form a standing wave. B) Velocity profile of the particle movement on the quartz surface.[34]

Lin and Ward[33] as well as Schneider and Martin[34] demonstrated by a simple experiment and theoretical treatment of the problem that indeed compressional waves are generated from the quartz surface and can be reflected at an interface. They mounted a reflector (glass plate), adjustable to the desired distance from the quartz plate (z-direction), several 100 μm away from the resonator. Both, the resonance frequency and the damping resistance *R* varied periodically with the distance of the reflector from the shear resonator. The periodicity was $\lambda_c/2$, in which λ_c represents the wavelength of the longitudinal wave in solution.

2.3.1.3. Conductance and Permittivity of the Solution

Other important parameters that influence the resonant frequency of the quartz crystal in solution are the ionic strength and dielectric constant of the electrolyte. Supposing that the operator of the QCM has to change the buffer conditions for a particular experiment an undesired parasitic frequency shift may occur, which can be more or less of the same magnitude as the measuring signal itself. This effect strongly depends on the shape of the electrodes and conductance of the solution. The series resonance shows only a minor response to changes in conductance and permittivity,[35] since all effects parallel to the motional branch add on the parallel resonant frequency of the crystal.[36] The parallel resonant frequency decreases with increasing conductance of the solution. An expanded BVD-equivalent circuit which explained the observations was first introduced by Shana and Josse.[37]

An additional parallel *RC* circuit (Figure 16B) has to be introduced to account for the influence of the conductance and dielectric constant of the medium. R_G can be neglected at high ionic strength, thus C_G and $C_{0,A}$ can be lumped into one capacitance to give the well-known BVD circuit with a modified capacitance C_0. Rodahl et al.[38] investigated the

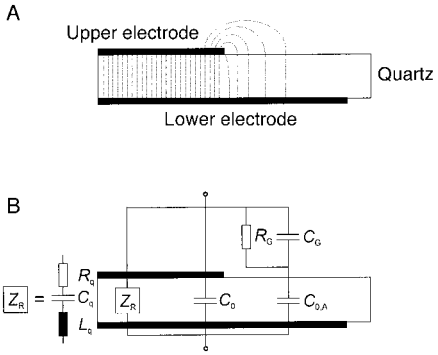

Figure 16. A) Course of the field lines at the electrode edges of a quartz oscillator. The origin of the changes in the quartz resonance frequency upon changing the ion conductance of the solution are field-fringing effects. B) These edge effects of the electric field can be represented by a *RC* element (R_G and C_G). As a result of the overlap of the electric field the effective area of the quartz is larger, hence the capacitance C_0 of the quartz is also increased by $C_{0,A}$.[37, 38]

influence of the conductance on the series and parallel resonant frequency as well as the damping of the resonator using differently shaped electrodes.[39] They found that field fringing is the predominant reason for changes in the resonant frequencies (Figure 16A). The extent of field fringing strongly depends on the shape of the electrodes. The strongest dependence of the parallel resonant frequency on the conductance of the electrolyte solution was seen for ring-shaped working electrodes in which the the center of the quartz resonator is not layered, for instance, while completely covered quartz plates do not display significant frequency shifts with changing conductivity.

2.3.1.4 Surface Roughness

Interpretation of adsorption phenomena is strongly influenced by the surface roughness of quartz resonators. In particular an alteration in the hydrophilicity upon adsorption can lead to tremendous changes in the resonant frequency. Rough and hydrophilic surfaces entrap liquids in small

cavities thus contributing to the overall mass detected by the device.[40, 41] Hydrophobic cavities, however, are often not wetted by the liquid and result in the inclusion of air or vacuum (Figure 17),[41] thus leading to smaller energy losses on hydrophobic surfaces than hydrophilic ones. This observation implies that the resonant frequency shifts to smaller values when changing from a hydrophobic to a hydrophilic surface. Hence, smooth surfaces are required when operating in fluids so as to avoid frequency shifts arising from changes in surface energies.

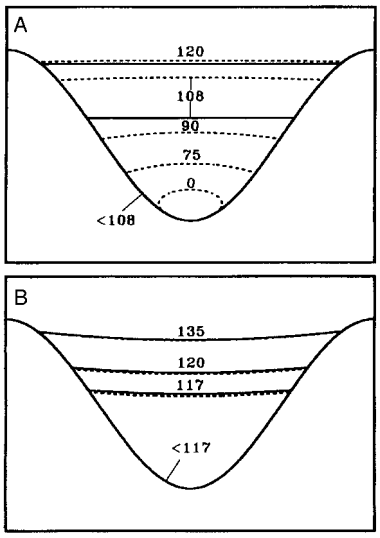

Figure 17. Cross-section of different liquid menisci formed in a sinusoidally textured surface illustrating contact angle dependent trapping (A) with trapped air and (B) without trapped air. The dashed lines indicate the initial penetration of liquid for the indicated microscopic contact angle. The solid lines indicate the equilibrium penetration, which becomes complete at $<108^\circ$ (A) and $<117^\circ$ (B).[7]

2.3.1.5. Electrochemical Double Layer

Tsionsky et al.[42] presented a consistent treatment of the influence of the electrochemical double layer on the resonant frequency. Considering the electrochemical double layer as a rigid mass on the basis of its extension of a few nanometers in the z-direction leads to an additional frequency change Δf_{DS}. The thickness of the double layer can be estimated to be about 1 nm for a 1:1 electrolyte of 0.1M. By taking into account that the extension of the shear wave of a 5 MHz quartz is 250 nm in water and therefore exceeds by far the thickness of the double layer this approximation holds for most cases. The influence of a thin rigid mass oscillating in phase with the resonator surface can be expressed by Sauerbrey's Equation. A change of the electrochemical double layer as a result of additional charges adsorbing to the surface leads to the following change in resonant frequency [Eq. (11a) and (11b)].

$$\Delta f_{DS} = -\frac{2f_0^2}{A\sqrt{c_{66}\rho_q}}\Delta m_{DS} \quad (11a)$$

$$\Delta m_{DS} = \frac{q_+}{F}(M_A - M_W n_A) - \frac{q_-}{F}(M_K - M_W n_K) \quad (11b)$$

M_A and M_K are the molecular masses of the corresponding anions and cations, M_W the molecular weight of water, n_A and n_K denote the number of substituted water molecules, and q_- and q_+ are the excess charges on the surface. Adsorption of positively charged particles on the resonator surface leads to an increase in adsorbed mass if it is assumed that sufficiently large counter ions are near the quartz. Therefore, charged particles can cause larger frequency shifts than uncharged ones. The influence of charges on the hydrodynamic properties of the adjacent water layer has not been considered yet.

2.3.1.6. Conclusion

In conclusion, interpretation of QCM data is not unambiguous and can lead to controversial results. The factors mentioned in Sections 2.3.1.2–2.3.1.5 have to be taken into account if conditions such as hydrophilicity, surface charges, meniscus, temperature, viscosity of the liquid, and buffer composition cannot be preserved. The QCM in fluids is not a simple mass-sensor but provides valuable information about interfacial reactions. Besides elasticity and viscosity, information about surface charges of biomolecules can be obtained. The following section gives an overview of other acoustic resonators.

2.3.2. Surface-Acoustic-Wave (SAW) Sensors

Lord Rayleigh was the first to discovered this acoustic mode known as surface acoustic waves (SAW). The stress-free boundary of a solid gives rise to these surface-confined waves that propagate as coupled longitudinal and transversal waves. The frequencies of SAW sensors are usually between 50 MHz and a few GHz.[7] The displacement components decay exponentially within the solid. The surface acts as an acoustic waveguide. Surface acoustic waves can be excited and detected by patterned interdigital transducers (IDT, see Figure 3) on the surface of single piezoelectric crystals such as quartz, lithium niobate, or lithium tantalate. Each "finger" is the origin of a surface acoustic wave. The transducer works most efficiently if the periodicity matches the wavelength of the surface wave occurring at $f = v_p/d$, in which v_p denotes the propagation velocity and d the distance between the interdigital fingers, that is, the periodicity. Generally, resonators can be distinguished as two port delay lines and one-port resonators.[43] Two port delay lines work with one IDT as a transmitter and one as a receiver. The separation between them determines the delay between the transmission and receiving of the surface wave. One-port resonators consist of one IDT structure in between two reflectors thus producing a standing wave in both directions. The resonant frequency is given by $f_n = n v_p/2l$, in which l is the distance between the reflectors. The quality factor Q of SAW devices is between 6000 and 12000 and is considerably lower than that of TSM resonators operating in air (20000–50000 for a 10 MHz fundamental frequency).

2.3.2.1. Mass Loading

If the deposited mass is a thin rigid film the kinetic energy of the synchronously vibrating system is increased without any energy loss arising from viscous damping. This then leads to a

decrease in the propagation velocity. The influence on the resonant frequency is given by Equation (12).[7]

$$\frac{\Delta f}{f} = \frac{\Delta v}{v_p} = -c_f^{SAW} f \rho_s \quad (12)$$

This equation resembles Equation (3). Again the mass sensitivity increases with the square of the fundamental frequency, which is considerably higher (> 100 MHz) than that of TSM resonators, and renders the sensitivity of a 100 MHz SAW sensor 200 times higher than the mass sensitivity of a 5 MHz quartz crystal. However, bioanalytic applications require operation in water, thus SAW sensors are less suited than TSM resonators as a result of the high energy loss occurring in an aqueous environment. Damping is a consequence of compressional waves generated by displacement components parallel to the surface normal and the viscous coupling of displacement components parallel to the surface.

2.3.3. Acoustic-Plate-Mode (APM) Sensors

APM sensors are cut from single-crystalline quartz to serve as acoustic waveguides that are particularly suited for operation in liquids. The acoustic wave is confined between the upper and lower surfaces of the plate propagating between input and output transducers, in contrast to SAW sensors in which they are restricted to one surface.[44] Shear-horizontal (SH) APM resonators do not exhibit displacement components parallel to the surface normal but predominantly display displacement parallel to the surface and the direction of wave propagation. Therefore, loss of acoustic energy from interaction with the environment is drastically reduced. The particle displacement has only one component.[45] SH modes can be considered as a superposition of plane waves with an in-plane (shear horizontal) displacement reflected at a particular angle between the upper and lower face of the quartz resonator. Similar to SAW sensors, acoustic waves can be excited and detected by lithographically patterned IDT metal structures (Figure 3). The input transducer with periodicity b and thickness d generates approximately the eigenfrequency calculated by Equation (13).[45]

$$f_n = \frac{v_p}{b}\left[1 + \left(\frac{n\,b}{2\,d}\right)^2\right]^{1/2} \quad (13)$$

2.3.3.1. Mass Loading

When the mass is strongly bound (nonslip boundary condition) to the surface the layer moves synchronously with the quartz surface. As a consequence the kinetic energy increases and the propagation velocity decreases as discussed previously for TSM and SAW resonators [Eq. (14)].[7]

$$\frac{\Delta f}{f} = \frac{\Delta v}{v_p} = -c_f^{APM} \rho_s \quad (14)$$

c_f^{APM} denotes the mass sensitivity, and ρ_S the surface mass density (mass/area on face) of the foreign mass layer.

2.3.4. Flexural-Plate-Wave (FPW) Resonators

FPW resonators are thin, rectangular membranes made of tension-free silicon nitride embedded in a frame of silicon that are manufactured photolithographically. Oscillations of these plates, which are only a few micrometers thick, can be excited piezoelectrically by IDT, electrostatically, or by using magnetic transducers. FPW resonators are characterized by a high quality factor and low energy loss in fluids at a low resonant frequency. Although the mechanical amplitude is rather high (100 nm) energy dissipation is low since the phase velocity of the acoustic wave is lower than the velocity of sound in most liquids (900 – 1500 m s^{-1}).[7] The low resonant frequencies (1 – 10 MHz) permit the use of low-cost electronics, thus providing an attractive alternative to the less sensitive TSM resonators. FPW devices can also be used as actuators for granular solids as a result of their high amplitude.

The simplest case of an oscillating isotropic plate includes an infinite set of waves known as Lamb waves.[46, 47] Two sets of waves can be distinguished: symmetric waves (S), with particle displacements symmetric about the neutral plane, and antisymmetric waves (A), whose displacements have odd symmetry. Only two waves, A_0 and S_0 (both of lowest order), occur in sufficiently thin plates. Notably, the phase velocity of the two waves differs tremendously. Thinner membranes exhibit lower phase velocities for the A_0 mode, in which the plate undergoes flexing as the wave propagates, while the phase velocity reaches its maximum value for the S_0 mode. In the case of the A_0 mode the eigenfrequency decreases with decreasing thickness of the membrane at a given wavelength λ [Eq. (15)].[7]

$$f = \frac{1}{\lambda}\frac{\sqrt{B}}{M} \quad (15)$$

B denotes the bending stiffness of the membrane[48] and M the specific mass of the membrane per unit area.

2.3.4.1. Mass Loading

Increasing the mass of the isotropic plate by a thin rigid layer of foreign mass results in a decreased phase velocity of the A_0 Lamb wave [Eq. (16)].[7]

$$\frac{\Delta f}{f} = \frac{\Delta v}{v_p} = -\frac{\rho_s}{2\,M} \quad (16)$$

The integral mass sensitivity $-1/2\,M$ can be increased by using thinner plates, thus reducing the phase velocity and hence the resonant frequency. A comparison of the different acoustic resonators is given in Table 4.

3. Adsorption of Biomolecules and Cells

3.1. Quartz-Crystal Microbalances

The core component of a quartz-crystal microbalance is the AT-cut quartz plate with fundamental resonance frequencies predominately in the range of 5 – 30 MHz. Since quartz plates with high fundamental frequencies are very thin and therefore difficult to handle, most quartz plates in use have fundamental

Table 4. Comparison of the different acoustic resonators. d = plate thickness; λ is the wavelength of the acoustic wave.

Resonator	d	Medium	f [Hz]	Example	Temperature stability	Mass sensitivity S_m[a] [(Hz/MHz)(ng/cm^2)$^{-1}$]
TSM	$\lambda/2$	g, fl	4 – 30	quartz 6 MHz, $d = 277$ μm $v_p = 3330$ m s^{-1}, $\lambda = 554$ μm	high	0.014 (6 MHz)
SAW	$\gg\lambda$	g	30 – 500	quartz 158 MHz, $d = 760$ μm $v_p = 3160$ m s^{-1}, $\lambda = 20$ μm	high/medium	0.20 (158 MHz)
SH/APM	$3 - 10\lambda$	g, fl	25 – 200	quartz 101 MHz, $d = 203$ μm $v_p = 5060$ m s^{-1}, $\lambda = 50$ μm	high	0.019 (101 MHz)
FPW	$\ll\lambda/2$	g, fl	2 – 7	ZnO 5.5 MHz, $d = 3.5$ μm $v_p = 550$ m s^{-1}, $\lambda = 100$ μm	medium	0.38 (5.5 MHz)

[a] $S_m \overset{\Delta m \to 0}{=} (\Delta f/f)1/\rho_s$.

resonance frequencies in the range of 4 – 10 MHz. Overtones are excited in order to obtain resonance frequencies larger than 15 MHz. Despite mechanical problems, very sensitive quartz crystals with fundamental resonance frequencies of about 30 MHz are also used.[49]

For the analysis of biomolecules and cells, measurements in fluids are required—particularly in aqueous solutions. By developing appropriate oscillator circuits capable of exciting AT-cut quartz crystals to their resonance frequencies under liquid load,[50, 51] the quartz crystal microbalance could be introduced as a powerful tool in life science. Up to now several quartz crystal microbalance setups have been realized:

a) A flow system comprising a quartz plate that is usually clamped between two O-rings. Since the radial mass sensitivity, described by a Gaussian function, decays towards the edges of the quartz plate it is advisable to minimize the contact area of the O-ring with the resonator and to place it as far outside the quartz as possible, so that damping is minimized and thus the quality factor is at a maximum. The measurement chamber has to be sealed to air to avoid air bubbles and alteration of the liquid meniscus in order to avoid reflection of induced longitudinal waves at the air – liquid interface which influence the resonance frequency of the quartz. An outlet and inlet of the quartz holder allows the addition of analytes at any given time while monitoring the resonance frequency. Apart from thermodynamic equilibrium values, kinetic data can also be obtained with this setup. The time resolution of the quartz crystal is limited by its quality factor and is in the range of milliseconds. Using a flow system ensures a proper mixing of the solution, so that rate-controlled kinetics might be assumed. Moreover, most setups can be fully automated for sensor applications.
b) A different approach to excite the quartz which has only one side in contact with liquids is to seal one side of the quartz with a rubber casing. Only one side is exposed to the fluid when the quartz is completely immersed into solution, with the other one kept in air. Addition of the analyte can be performed using a syringe while stirring the solution continuously.
c) Further techniques to immerse quartz crystals with only one side in aqueous solution are based on moving a quartz plate horizontally at the air – water interface; beforehand, a film is spread at the air – water interface and compressed to the desired film pressure. In this way, the quartz plate is in close contact with the monolayer. Upon addition of the analyte into the subphase, the interaction can be monitored.
d) The simplest approach is to monitor frequency shifts in air after adsorption of the biomolecules in fluids and drying of the surface. This technique allows only the determination of final frequency values with large errors arising from the continuous change between air and liquid. The resonance frequencies obtained vary considerably compared to those gathered from measurements in liquids, since the water content of the biomolecules influences the response of the quartz significantly. The only advantage of this technique is given that the Sauerbrey Equation might be valid under these conditions.
e) Inspired by the finding that the vibration of the quartz is considerably influenced by a liquid, the so-called reference crystal method has been developed. With this setup, two quartz crystals are excited in parallel. One of the surfaces of the two quartz crystals is functionalized while both of them are immersed in the same medium. This results in a net detection of the biomolecules. However, this method is not frequently used since other disadvantages occur from the different surfaces of the two crystals which lead to temperature and resonance frequency instabilities.

There are basically two different modes of operation for TSM resonators. One is based on the quartz crystal being the frequency-determining element of the oscillator circuit. The surface coverage of the quartz can be obtained by monitoring the resonance frequency. The read out of the resonance frequency is routinely performed using an oscillator circuit connected to a frequency counter. This mode of operation is termed active, since the crystal is excited to its resonance frequency and the oscillator circuit compensates for the energy loss. One should keep in mind that the exact resonance frequency that is excited by the oscillator circuit is not necessarily known so that experimental results might not be comparable using different oscillator circuits. Especially, if energy dissipation as a result of viscoelastic load occurs then frequency responses can be quite different. The equations depicted in Table 2 outline the various resonance frequencies of a moderately damped system to demonstrate this problem.

Therefore, it is important to know whether the serial or parallel resonance is supported by the oscillator circuit. However, the feedback of the oscillator circuit often introduces inevitable phase shifts, which result in considerable deviations from the serial or parallel resonance so that an accurate determination of the excited resonance frequency remains difficult.

The other mode of operation, the so termed passive method, uses a network analyzer/frequency generator to excite the crystal to a constraint vibration near resonance while monitoring the complex electrical impedance or admittance dependent on the applied frequency. By fitting the parameters of the BVD-equivalent circuit to the spectra (Figure 6B) both the mass load and energy dissipation can be determined separately.

A connecting link between simple frequency determination and complex network analysis is the so-called QCM-D technique developed and commercialized by Kasemo and co-workers,[52] which allows the resonance frequency and dissipation factor to be monitored simultaneously. In this technique a quartz plate is excited with a frequency generator followed by switching off the source and recording the free decay of the quartz oscillation. This procedure is repeated each second. The dissipation factor together with the resonance frequency is obtained by a curve fit. Damping can also be recorded using an amplitude-controlled oscillator circuit that monitors the amplitude separately from the resonance frequency.[53]

3.2. In Situ Hybridization of DNA/RNA on Quartz Surfaces

The analysis of genetic material, such as that essential for the diagnosis of hereditary and infectious diseases, for the classification of an organism, and in the field of forensic chemistry, has attained enormous importance and has led to numerous techniques to quantify nucleic acids in a sensitive, selective, and fast manner, that is, high-throughput screening. In the course of these developments mass-sensing devices were included in the repertoire of signal transducers that are capable of detecting oligonucleotides label-free and online. The first evidence of a direct measure of nucleic acids using an acoustic resonator was given by Fawcett et al.;[54] however, the experiments were performed in air. The first in situ experiment was accomplished in fluids using an acoustic-plate-mode resonator[44] and the second one with a thickness-shear-mode resonator, which was functionalized with a single-stranded DNA coupled through a self organized 11-sulfanylundecanol monolayer chemisorbed on gold.[55]

The crucial step in developing a mass-sensitive nucleic acid detecting device is the immobilization of a single-stranded oligonucleotide on the resonator surface which hybridizes selectively with the complementary strand from solution. Well-known procedures are the modification of 5′-phosphate residues by thiol groups.[56–60] In this way, DNA as well as RNA can be immobilized, and also peptide nucleic acids carrying a polyethylene-modified terminal cysteine.[61] Suitable procedures solely for DNA and RNA are based on electrostatic interactions of the negatively charged backbone and positively charged amine monolayers.[62, 63] Frequently used methods, though quite complicated, are based on the binding of biotinylated oligonucleotides to surface-confined avidin or streptavidin. The coupling of proteins is accomplished by simple physisorption,[64] by electrostatic interaction,[63] or covalently linked through an amide bond between chemisorbed 3,3′-bispropionic acid and the amine residue of the protein.[56, 65, 66] Unfortunately, the oligonucleotide coverage is not well determined in most cases; surface coverages are mostly calculated after adsorption of the nucleic acid in air or liquid using the proportional constant of the quartz as determined before. The average values obtained are well below 100%, with typical coverages between 10 and 30%. A correct correlation between the actual concentration of the nucleic acid at the surface and the frequency decrease, as experimentally determined by Su et al.,[67] demonstrated that the surface coverage obtained from the frequency shift is 3 to 12 times larger than that determined by radioisotope labeling. The question is whether the common oligonucleotide immobilization techniques provide satisfactory surface coverages. The quality of the immobilization method is rather important for dealing with aspects such as sensitivity and specificity since the surface coverage reflects the sensitivity of the mass-sensing device. Moreover, nonspecific adsorption can be minimized by complete surface coverage. A desirable, user-demanded detection limit is approximately 10^{-18} M, but depends on the number of base pairs.[68] In order to minimize the detection limit of a functionalized resonator surface quartz crystals with higher resonance frequencies were used, multilayers composed of nucleic acids and polymers/proteins were developed,[63] DNA dendrimers were synthesized,[69] and nucleic acids were amplified on the surface by using the polymer chain reaction (PCR).[70] In a recent study Bardea et al.[71] used anti-double-stranded DNA and anti-mouse F_c antibodies as a second antibody to amplify the signal. Despite these efforts, the detection limit is currently in the range of 10^{-8} – 10^{-7} M.[56, 60, 69]

Besides difficulties of nucleic acid immobilization and sometimes unknown surface coverage the reason for a low detection limit can also be sought in the low hybridization yields on the surface, which do not exceed 10%.[57, 59, 67] Steric hindrance of the hybridization reaction explains this low value; however, the equivalence of mass change and frequency upon the detection of nucleic acids in solution is questionable. Although the translation of the frequency shift into mass using the Sauerbrey Equation is pursued in many publications, one should refer to the articles of Thompson and co-workers[67, 72–74] and Fawcett et al.,[68] who showed that oligonucleotides immobilized on the resonator surface in fluids do not behave like an ideal rigid mass. Thompson and co-workers revealed, for example, that the serial resonance f_s upon binding of DNA exhibits a frequency change which is 18 times larger than predicted by the Sauerbrey Equation. They attributed this discrepancy to an altered viscosity on the surface that was generated by hybridization. Network analysis revealed that the motional resistance R, which is indicative of energy loss, changes in the same fashion as the serial resonance frequency. For immobilized DNA, R is not only

dependent on the liquid's viscosity but is also influenced by the electrolyte effecting the electroacoustic coupling of the oscillation. Thus, R is additionally determined by the solution's conductivity and the electrochemical double layer, which makes a particularly large contribution in the case of highly charged DNA.[67] These altered viscoelastic effects can be used to obtain kinetic data of the DNA hybridization on the surface.[72] However, a systematic study remains to be performed.

Besides sensitivity, the specificity of oligonucleotide biosensors is also of paramount importance. Bardea et al.[60, 71] showed, that a seven base pair mutation within a 31-mer that occurs in the genome of the Tay–Sachs disease is sufficient to inhibit hybridization of the mutated DNA with surface-immobilized complementary strands. In contrast, 10-mers containing two terminal mutations hybridize almost completely (92%), while DNA with one mutation positioned in the center of the strand hybridizes with a yield of only 30%. However, nonspecific adsorption of oligonucleotides could not be excluded.[57] An increased sensitivity was gained by using peptide nucleic acids instead of DNA on the surface. Functionalization of gold surfaces with peptide nucleic acids has the effect that a single point mutation of the complementary DNA strand is sufficient to inhibit DNA binding to the surface (Figure 18).[61]

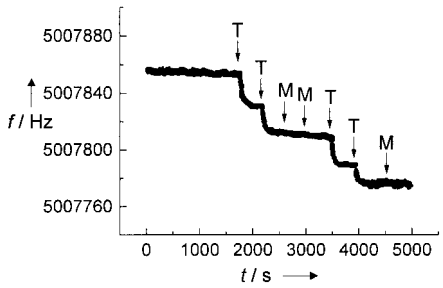

Figure 18. Frequency-time response of a QCM biosensor functionalized with a peptide nucleic acid of the sequence Cys-egl-GGC-AGT-GCC-TCA-CAA for multiple additions of 10 μg mL^{-1} of the 15-mer 5′-TTG-TGA-GGC-ACT-GCC-3′ (T) and of 50 μg mL^{-1} of 5′-TTG-TGA-G**A**C-ACT-GCC-3′ (M). The mismatch base is indicated in bold.[61]

A recent study of Wang et al.[75] illustrates the use of the quartz-crystal microbalance to monitor real-time enzymatic activity of RNAses and DNAses using surface-confined poly(U) single strands and $(dA)_{20}-(dT)_{20}$ double strands. The specificity of both enzymes was preserved on the surface.

3.3. *Adsorption of Proteins at Functionalized Surfaces*

The primary area of application of the quartz-crystal microbalance today is the investigation of protein adsorption at functionalized surfaces. For instance, the basic principle of piezoimmunosensors is the detection of the binding of antibodies to surface-confined antigens. For a long time it was postulated that a direct quantification of the adsorbed amount of protein would be feasible by using the Sauerbrey Equation. However, a number of publications established that protein adsorption performed in liquid leads to larger frequency shifts than in air. In order that the quartz-crystal microbalance can be used as a universal tool it is desirable to find reasons for the different frequency changes. A study from 1993 found for the first time a direct correlation between mass load and frequency shift by adsorbing human serum albumin (HSA) on the resonator.[76] Muratsugu et al. quantified the mass load by using radioisotope-labeled HSA in combination with the determination of the frequency shift by using the quartz-crystal microbalance. This result is a hallmark with respect to the sensitivity of shear-wave resonators. While $\Delta f/\Delta m$ is supposed to be 0.183 Hz cm^2 ng^{-1} for a 9 MHz quartz as predicted by Sauerbrey, the results revealed values of (0.375 ± 0.012) Hz cm^2 ng^{-1} for HSA and a value of (0.716 ± 0.066) Hz cm^2 ng^{-1} for anti-HSA. On the one hand, these numbers are considerably larger than that expected from the Sauerbrey Equation, and on the other hand, they depend on the investigated protein. In order to clarify this discrepancy, Kasemo and co-workers developed a measuring device that allowed frequency shifts to be monitored simultaneously with energy loss, which was represented as the dissipation factor with a time resolution of 1 s.[52] Energy loss can occur within the adsorbed film, where included water also has to be taken into account, or at the interfaces as a result of friction. Their experimental results in aqueous solution confirmed that energy loss, that is, an increase in the dissipation factor, can be detected.[77–79] Thus, binding of methemoglobin (met-Hb) and hemoglobin-CO (HbCO) on a hydrophobic methyl-terminated monolayer exhibits the expected frequency decrease as well as an alteration of the dissipation factor D (Figure 19A, B). Plotting the frequency shift versus change in D gives rise to two distinct slopes, which indicates that a two step adsorption process occurs (Figure 19C).

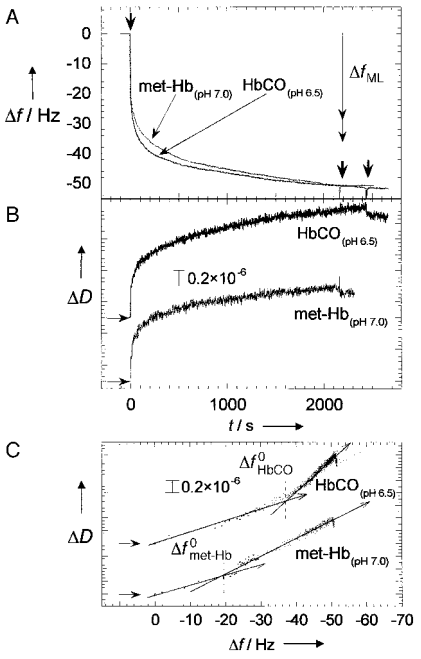

Figure 19. A) Changes in frequency and B) dissipation as a function of time during the adsorption of met-Hb and HbCO at pH 7.0 and pH 6.5, respectively, onto a methyl-terminated thiol monolayer (ML). C) Plot of the change in the dissipation factor versus the change in frequency. Two different slopes, which indicate a two-step adsorption process, are discernable for the adsorption of both met-Hb and HbCO.[78]

These results have led to the conclusion that energy loss does not only occur at the interfaces but also in the protein layer itself; dissipation might be attributed to conformational changes within the adsorbed protein layer and tightly bound water; they are induced by periodic shear movement. The hypothesis that enclosed water contributes considerably to the frequency shift was confirmed by Rickert et al.[80] Upon deposition of multilayers composed of alternating layers of biotinylated BSA and streptavidin they obtained a sensitivity that was four times larger than the integral mass sensitivity as predicted from the Sauerbrey Equation. By determining the thickness of the layer they could demonstrate that approximately 75% of the overall mass is water. They excluded viscoelastic effects since a nonchanging frequency shift per protein layer up to 20 monolayers was observed. A decrease in the frequency response by a factor of approximately 0.7 would be expected according to Rickert et al. if the protein layer showed viscoelasticity.[80]

Although the frequency shift cannot be translated into mass load, it is nevertheless conceivable that the quartz-crystal microbalance could be used for in situ measurements of binding events. Concentration-dependent measurements of the frequency shift together with the assumption of a linear relation between frequency shift and mass load allow the binding and rate constants of the protein and peptide adsorption to be determined.[66, 81–85] The technique is well suited for the quality control of multilayers prepared by the Langmuir–Blodgett technique[86] or self-organization processes.[80, 87–94]

3.4. Lipid–Protein Interactions at Solid-Supported Lipid Membranes

Protein–receptor interactions at lipid membranes, for example ganglioside–toxin interactions play an essential role in biological processes. The first contact of a protein, virus, or bacterium with its receptor at a biological membrane initiates a variety of reactions at the cell membrane. Artificial membrane systems which are variable in their lipid composition are necessary for investigating these kind of interactions at a lipid membrane.[95, 96] Nowadays, common model membrane systems are vesicles and black lipid membranes. Lipid membranes immobilized in a highly ordered fashion on solid supports are of great interest for the quartz-crystal microbalance. Different preparation techniques are available to prepare so-called solid-supported membranes. The Langmuir–Blodgett and Langmuir–Schäfer techniques, for example, allow the transfer of highly ordered lipid monolayers from the air–water interface onto a pretreated quartz surface. Instead of using these equipment-intensive methods, techniques based on the chemisorption of thiol or disulfide components are well suited for immobilizing lipid bilayers on gold-covered quartz plates. In a first step gold surfaces are functionalized using sulfur-containing components. These self-organized monolayers serve as starting points for the preparation of lipid bilayers. Common methods for the preparation of lipid bilayers are the vesicle-fusion technique, detergent dilution method, or painted lipid membrane procedure.[96]

Okahata and co-workers[97–100] immobilized lipid monolayers at the air–water interface of a quartz surface by dipping it horizontally from the air-side at the interface. The hydrophilic head groups are oriented towards the water subphase so that proteins and peptides dissolved in the subphase may interact with them. These functionalized quartz plates allowed the binding and dissociation constants of the interaction of melittin and β-globulin with dipalmitoylphosphatidylethanolamine membranes to be determined; moreover the binding of the lectine concanavalin A to glycolipid monolayers was quantified.[101] It is very easy to incorporate various numbers of receptor molecules in those lipid monolayers at the air–water interface. With the same preparation technique it was feasible to investigate the binding behavior of the influenza A virus and wheat germ agglutinin with G_{M3}-doped monolayers composed of sphingomyeline and/or glucosylceramide. Variation of the lipid matrix and the dopant concentration revealed that only these parameters are pivotal for virus binding and that the binding rate is influenced considerably. The system allows the inhibition of the virus binding by adding sialyllactose (Neu5Ac-α-2–3Gal-β-1–4Glc).[97, 99, 100, 102]

The above-mentioned methods based on the self-organization of lipids on surfaces make it possible to readily prepare lipid membranes that are composed of two single leaflets. A lipid bilayer composed of a first chemisorbed alkanethiol monolayer and a second lipid monolayer can be obtained by fusing unilamellar vesicles on the hydrophobic monolayer. These vesicles fuse on the surface so that their composition also determines that at the surface. Impedance analysis of the mono- and bilayers allows an exact quality control of each layer, thereby ensuring highly reproducible membrane preparations (Figure 20).

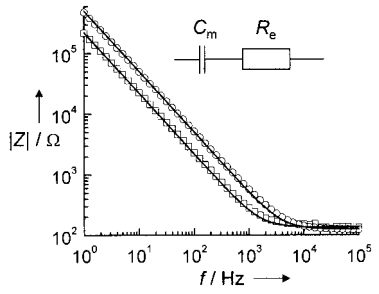

Figure 20. Impedance spectra of an octanethiol monolayer (□) and a lipid bilayer composed of octanethiol and 1-palmitoyl-2-oleoyl-*sn*-glycero-3-phosphocholine (POPC; ○). The solid lines show the results of fitting the parameters of the simple equivalent circuit depicted.[103]

A comparison of two different QCM investigations demonstrates that the choice of the artificial membrane system significantly influences the obtained results. Both studies dealt with the adsorption of melittin to phospholipid membranes. Whereas Okahata and co-workers used lipid monolayers at the air–water interface and obtained an ideal Langmuir adsorption isotherm for melittin concentrations of up to 100 μM,[100] Steinem et al.[103] used lipid bilayers and

obtained adsorption isotherms which indicated multilayer adsorption started at a concentration of 8 μM. The immobilized membrane was solubilized by melittin at concentrations larger than 20 μM, these effects were not observed at the air–water interface.

In principle, the quartz-crystal microbalance in combination with lipid membranes composed of an alkanethiol monolayer and a second lipid monolayer obtained by vesicle fusion allows an easy determination of thermodynamic and kinetic parameters of protein–ligand couples without the use of labels. The example of the interaction of peanut agglutinin (PNA) with gangliosides shows the suitability of this approach. A lipid membrane is doped with different concentrations of the receptor lipid G_{M1} and the frequency shift is monitored upon addition of PNA. Figure 21 shows that a dopant concentration of 1.3 mol% of the receptor lipid G_{M1} is sufficient to achieve maximum coverage of the protein

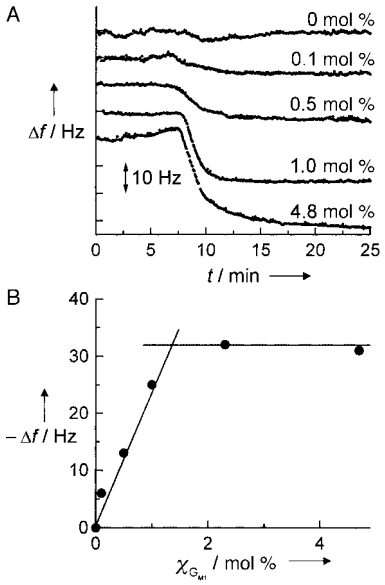

Figure 21. A) Frequency shifts of a 5 MHz quartz functionalized with solid-supported octanethiol/POPC lipid bilayers containing different amounts of G_{M1} upon addition of 2 μM of PNA. B) Dependence of the equilibrium value of the resonance frequency Δf on the mole fraction $\chi_{G_{M1}}$ within the phospholipid monolayer. The solid lines intersect at $\chi_{G_{M1}} = 1.3$ mol%.[107]

surface. A calculation of the theoretical value of the minimum number of necessary G_{M1} molecules within the lipid matrix, assuming a homogenous distribution of the receptor lipids and correct values for the geometry of the protein, leads to a value of 1.5 mol%. A comparison of the theoretical value with the one obtained experimentally implies that the monomeric protein coverage on the surface has to be close to one. Similar maximum protein coverage using a lipid matrix doped with 2 mol% of the receptor lipid was corroborated by Ebato et al.[104] who investigated the streptavidin–biotin couple with the quartz-crystal microbalance. The frequency shift Δf has to be monitored at various concentrations of the protein c_0 in solution to determine the binding constant of a protein–receptor couple (Figure 22). By assuming that the binding sites on the surface are energetically equivalent and that there is a

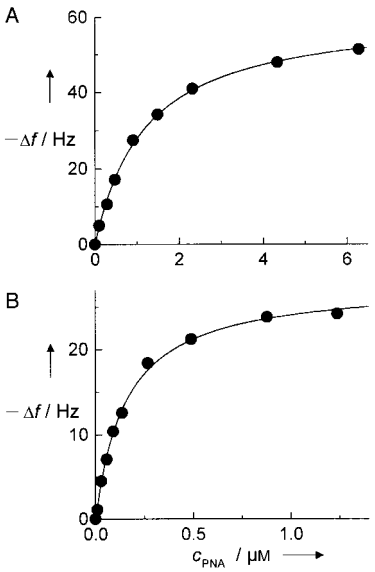

Figure 22. Isotherm of the binding of PNA to a G_{M1}-doped lipid bilayer (A) and to an *asialo*-G_{M1}-doped octanethiol/POPC bilayer (B) immobilized on a gold-covered AT-cut quartz. The dependence of the equilibrium resonance frequency shift Δf on the PNA concentration in solution is shown. The POPC monolayer was doped with 4.8 mol% of the receptor lipid. The solid line is the result of fitting the parameters of a Langmuir isotherm according to Equation (17) with $K_a = (0.8 \pm 0.1) \times 10^6$ and $(6.5 \pm 0.3) \times 10^6\,\mathrm{M}^{-1}$, respectively, and $\Delta f_{max} = -(61.0 \pm 0.5)$ and (28.0 ± 0.5) Hz, respectively.[109]

homogeneous distribution of the receptor lipids,[105] the binding constant K_a can be obtained by fitting the parameters of a Langmuir adsorption isotherm [Eq. (17)] to the data.

$$\Delta f = \Delta f_{max} \frac{K_a c_0}{1 + K_a c_0} \qquad (17)$$

The established binding constants present information about the chemical structure of the receptor essential for an appropriate binding, as demonstrated by the adsorption of PNA to G_{M1} and *asialo*-G_{M1}. While the binding constant of PNA to G_{M1} is $K_a = (0.83 \pm 0.04) \times 10^6\,\mathrm{M}^{-1}$, it is determined to be almost a factor of 10 larger at $K_a = (6.5 \pm 0.3) \times 10^6\,\mathrm{M}^{-1}$ for *asialo*-G_{M1}.[105] This difference is attributed to the fact that *N*-acetylneuramic acid of G_{M1} is not necessary for or even disrupts the binding of PNA. However, it has been demonstrated that the affinity of PNA to the trisaccharide β-Gal*p*-(1,3)-GalNac-(1,4)-β-Gal*p* is larger than to the dissaccharide β-Gal*p*-(1,3)-GalNac.[106]

This is an example how the molecular structure of a receptor molecule can be illuminated by varying the receptor molecules embedded in the lipid membrane using the quartz-crystal microbalance. Besides quantifying the inhibition of binding in solution this method is capable of clarifying carbohydrate structures that play a pivotal role in receptor function. Monitoring the frequency shift upon binding of PNA to G_{M1} in the absence of an inhibitor (Figure 23) allows the binding constant K_I of the inhibitor in solution to be determined.[107] A prerequisite for the determination of K_I is an appropriate ratio between K_I and K_a. If the binding constants have similar orders of magnitude an exact determination of the binding constant K_I is practicable since the

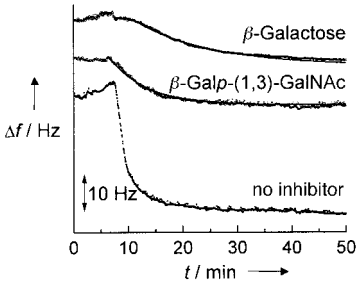

Figure 23. Time course of the resonance frequency shift upon addition of a 2 μM solution of PNA to a lipid bilayer composed of octanethiol and POPC doped with 4.8 mol % of G_{M1} without inhibitor, with 0.27 mM β-Galp-(1,3)-GalNAc, and 26.5 mM β-galactose.[107]

frequency changes continuously with the inhibitor concentration in solution. If there are several orders of magnitudes between K_I and K_a, the protein binds either almost unaffectedly on the surface or not at all.

The PNA – ganglioside system displays the potential of the quartz-crystal microbalance combined with solid-supported membranes in regard to studying ligand – receptor couples and the parameters which can be calculated from the obtained data. In summary, it can be concluded that the QCM technique enables one to quantify binding constants and kinetics in a relatively simple fashion so that information can be gathered about the structure of natural receptor molecules. This feature was particularly demonstrated in a study dealing with the adsorption of bacterial toxins—cholera, tetanus, and pertussis toxin—on various gangliosides.[104, 107–109]

Besides basic knowledge that can be garnered from lipid membranes immobilized on quartz crystals, this system might also be useful for biosensor applications. Solid-supported lipid membranes on gold surfaces are not only well-suited because they can be prepared reproducibly with an exactly adjustable composition, but also because they are of particular interest, since nonspecific protein adsorption arising from the lipid matrix is strongly suppressed. First experiments pointing in the direction of regenerating the sensor surfaces after binding of a protein were demonstrated by Janshoff et al.[107] Upon addition of protease, the adsorbed protein can again be released from the surface (Figure 24).

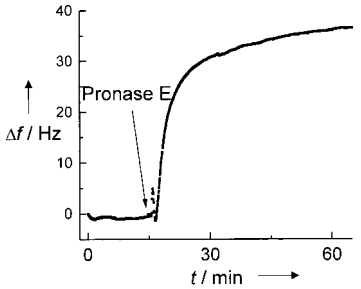

Figure 24. Time course of the resonance frequency shift upon addition of a pronase solution to a PNA-covered lipid bilayer composed of octanethiol and POPC doped with 4.8 mol % of G_{M1}. The PNA concentration was 2 μM, the concomitant frequency shift −36 Hz. The concentration of pronase E was 0.2 % (w/w). The frequency increase arising from the action of pronase was 35 Hz after incubation of the protein monolayer in solution for approximately 1 h.[107]

3.5. Piezoimmunosensors

The high specificity of antigen – antibody reactions and the ability to generate antibodies against a variety of biological and nonbiological substances opened up a way to develop immunosensors to address questions in areas ranging from clinical diagnosis, food control, to environmental analysis. During the last three decades radioisotope-labeled antibodies were mostly used for immunoassays.[110] Disadvantages that emerge from work with radioactive components has led to the development of new marker systems, that is, fluorescence-labeled antibodies. Nowadays the enzyme-linked immunosorbant assay (ELISA) is the most widespread analysis tool to detect antibody – antigen reactions. The peculiarity of this detection method is the amplification of the antigen – antibody reaction using an enzyme that is bound to the antibody and catalyzes a detectable reaction, namely, the formation of a UV/Vis-active or fluorescence active dye.[111] Despite this established technique, interest in discovering label-free and less time consuming online detection methods is still undiminished. Numerous articles were published dealing with the immobilization of antibodies or antigens on transducer surfaces whose signal is affected upon binding of the complement. Such immunosensors are valued with respect to their handling, their overall costs, and how the sensor surface can be recycled without loss of sensitivity.

Piezoelectric immunosensors, such as the quartz-crystal microbalance and SAW sensors, are suitable transducer surfaces which fulfill the above demands appropriately. Piezoelectric immunosensors in the gas phase have been investigated for quite some time[112–116] whereas the online detection of antibody – antigen reactions in aqueous solutions originally started with the work of Roederer and Bastiaans on SAW sensors[117] and Thompson et al.[118] on AT-cut quartz plates. Contradictory to the classical understanding of piezoelectric sensors Thompson and co-workers found a frequency increase upon binding of immuglobin G (IgG) to the immobilized antigen in their first study. They concluded from this result that an alteration of the microviscosity at the interface was induced upon binding of the antibody.

Similar publications from this time also dealing with the piezoelectric detection of IgG established, however, that a frequency decrease was observed upon the binding of an antibody; hence the previously published frequency increase remains questionable.[119, 120] All further studies supported the decrease in frequency upon the binding of an analyte to a surface.

Nowadays the applicability of piezoimmunosensors to various fields has been proved. The spectrum ranges from medical applications for the detection of bacterial toxins[121–123] and viruses[114, 116, 124–128] through the determination of bacteria[55, 115, 129–132] in the food industry, to environmental analysis for the detection of organic compounds by using an antigen – antibody reaction.[122, 133–137]

For the development of a functional bioimmunosensor based on piezoelectric transducers, problems characteristic to all biosensors need to be solved: 1) functionalization of the electrode-covered surface, 2) sensitive, specific, and reprodu-

cible detection of the analyte in solution, and 3) regeneration of the sensor surface.

The immobilization technique of antigens or antibodies regularly leads not only to a functionalized sensor surface but also determines substantially the sensitivity and reproducibility of the sensor. A frequently used method is based on the simple physisorption of the desired compound on clean gold surfaces[120, 124, 126–128, 131, 138, 139] and polymers.[88, 115, 140] The stability of those immobilized molecules does not differ significantly from covalently coupled ones.[129, 132, 138, 141, 142] However, problems arising from these techniques are the nondirectional orientation of the molecules on the surface, namely, that part of the antigens/antibodies is not accessible. An oriented immobilization of antibodies can be achieved by nonoriented physisorption of antibodies or covalent coupling of protein A followed by an oriented adsorption of the antibody through the F_{ab} domain. Thus, the F_{ab} domain points preferentially to the external medium.[114, 119, 120] Another possibility is to utilize the linkage of the antibody to an individual thiol group.[143] In this way Göpel and co-workers succeeded in the arranged linkage of an antigen—a synthetic peptide of the mouth and claw epidemic virus—on a ω-hydroxyundecanethiol monolayer.[87, 144, 145] Another technique for the oriented immobilization of antibodies using Langmuir–Blodgett films with F_{ab} fragments bound to linker phospholipids was successfully demonstrated by Vikholm et al.[143, 146]

However, a major problem remains: the nonspecific adsorption at the transducer surface that can only be minimized by improved immobilization techniques and cannot be influenced by the transducer itself. The functionalized surface is often blocked with a protein such as BSA or casein before the binding of the analyte so as to minimize nonspecific adsorption. Additionally, nonspecific adsorption, which is predominantly caused by hydrophobic interactions, can be reduced by the addition of detergents.[124, 126, 128]

Apart from nonspecific interactions, which generate undesired signals independent of the choice of the transducer, viscous coupling of the liquid can cause severe problems if the solution's composition is varied during the experiment. The shear-wave resonator responds sensitively to variations in the solution's properties, namely, an altered viscosity. There are several possible ways of minimizing this bulk effect. If the viscosity of the solution under investigation is known, the viscosity of the medium can be adjusted by adding an appropriate amount of glycerol.[128] Aberl and co-workers used diluted humane serum albumin as a medium to minimize nonspecific adsorption.[124, 126] More general procedures to prevent this problem, which do not require the knowledge of the solution's composition, are the reference crystal method[147] and the same-condition method.[148] A new procedure was introduced by Zhang et al.,[149] after they were able to distinguish the mass load of the quartz from viscoelastic effects by measuring the resonance frequency and the amplitude of the applied voltage simultaneously. The obtained frequency shift could be corrected by viscoelastic effects with this setup.

The minimization of nonspecific adsorption enhances the sensitivity of the piezoelectric immunosensor. Furthermore, the minimum concentration which can still be detected with this method is determined by the binding constant of a given ligand–receptor couple. Ebato et al.[135] showed that the immobilization of an antigen (fluoresceine-labeled lipid) decreases the binding constant on the surface by a factor of 300 relative to the reaction in solution.

Eventually, the question remains as to whether the surface can be regenerated after the binding of the analyte and allow further binding studies. Willner and co-workers used a reversible cleavage of antibodies which were bound to an antigen-covered gold surface of a shear-wave resonator. They functionalized gold surfaces of 9 MHz quartz plates with the photoisomerable substrate *N*-methyldinitrospiropyran, which exhibits an affinity to the antibody antidinitrophenyl-Ab. Light with a wavelength of $360\ \text{nm} < \lambda < 380\ \text{nm}$ induced an isomerization of *N*-methyldinitrospiropyran to *N*-methyldinitromerocyanin, which does not exhibit an affinity to the antibody. The resiomerization occurs at $\lambda > 495\ \text{nm}$. The reversible binding of the antidinitrophenyl-antibody was impressive as demonstrated by QCM measurements.[150–152] Another technique to achieve reversible antibody–antigen interactions at surfaces was presented by Sargent and Sadik.[140] They immobilized anti-HSA antibodies on a conductive polypyrrole surface on a quartz plate and were able to induce a reversible binding by applying voltage steps.

In summary, piezoelectric immunosensors are an alternative to established ELISA methods. In contrast to ELISA techniques, which need a marker molecule and take approximately two hours, this method can be fully automated. Nowadays, the quartz-crystal microbalance provides a technique for analyzing phage libraries within a short time by using a flow injection system.[153] The detection of the analyte can occur online and is label-free within 10 min; moreover, kinetic data can also be used to specifically detect an antibody. The specificity is determined predominately by the chosen immobilization techniques and is therefore equivalent for ELISA and quartz crystal microbalance measurements. However, as yet the obtained sensitivity of piezoimmunosensors is lower than that of an ELISA assay.

3.6. Detection of Cellular Systems

The application of microgravimetric acoustic sensors for the detection and characterization of pro- and eukaryotic cells has led to a number of interesting experimental findings as a result of the abundant information provided by such an analysis. Complex and time-consuming methods of cell biology may one day be replaced by faster, more highly resolving, and simpler techniques using TSM resonators as piezoelectric sensors. These sensors are particularly important in the food industry for the routine determination of bacterial cell numbers in diets, but it is also desirable in clinical areas to be able to determine cell numbers in body fluids online. Table 5 gives an overview of bacteria whose cell numbers were determined using piezosensors.

Most piezosensors used for the detection of bacteria in solution are based on antigen–antibody reactions in which the bacterium binds to the corresponding surface-confined antibody and thus can be monitored. In this way, the highest

Table 5. Summary of cell types that were investigated using quartz resonators. The lowest detection limit as well as the surface reaction that was used for detecting the cells are given.[186]

Cell species	Cell number[187]	Surface reaction
Staphylococcus epidermidis[187]	$1 \times 10^2 - 4 \times 10^7$ cells mL^{-1}	liquidation of gelatin
Listeria monocytogenes[131]	$2.5 \times 10^5 - 2.5 \times 10^7$) cells per quartz	antigen – antibody
Chlamydia trachomatis[129]	0.26 – 7.8 $\mu g\,mL^{-1}$	antigen – antibody
Vibrio cholerae[122]	$> 10^5$ cells mL^{-1}	antigen – antibody
Candida albicans[188]	$10^6 - 5 \times 10^8$ cells mL^{-1}	antigen – antibody
Enterobacteriaceae[189]	$10^6 - 10^9$ cells mL^{-1}	antigen-antibody
Salmonella typhimurium[190]	$10^5 - 10^9$ cells mL^{-1}	antigen – antibody
Salmonella typhimurium[132]	$9.9 \times 10^5 - 1.8 \times 10^8$ CFU mL^{-1}[a]	antigen – antibody
Salmonella typhimurium[191]	$3.6 \times 10^6 - 102 \times 10^6$ cells mL^{-1}	cell growing on SS-agar[b]
Pseudomonas cepacia[192]	$> 3 \times 10^5$ cells cm^{-2}	cell growing on gold
Staphylococcus epidermidis[193]	3.9×10^{-2} % (v/v)	antigen – antibody, agglutination in solution
Pseudomonas aeruginosa[130]	$10^5 - 10^8$ cells mL^{-1}	antigen – antibody

[a] CFU = colony-forming unit (number of cells in a culture that can build a new colony in a layer). [b] SS = *Salmonella shigella*.

specificity is ensured. However, problems similar to those of immunosensors occur, such as nonspecific adsorption, which can only be abolished by blocking the free binding sites prior to the binding assay. In most cases a linear correlation between the bacterial cell number and frequency shift can be found, thus enabling one to calibrate the system for bacterial cell numbers. These studies are based on the assumption that the frequency shift upon cell binding can be attributed to a simple mass change as described by the Sauerbrey Equation. However, in 1993 Gryte et al.[154] and Redepenning et al.[155] were the first to point out that cells on quartz resonators in a medium cannot be treated like an ideal rigid mass. Cells are more likely to be presented as a viscous load similar to a fluid. A single cell layer on a 5 MHz quartz would give rise to a theoretical frequency shift of 5600 Hz according to the Sauerbrey Equation.[155] The actual values are in general at least one order of magnitude lower than that. This observation is attributed to the concept that a cell body behaves like a viscoelastic body (for example, Voight or Kelvin body)[156] under shear stress, which leads to the fact that besides an increase in the kinetic energy as a result of a mass change (increase in inductance L) an energy dissipation (increase in R) also occurs. It was shown that the shear wave within the system composed of the cell, extracellular matrix, and a water layer vanishes. This result was confirmed by experimental results in which cell multilayers and the adsorption of silica beads do not cause a detectable frequency shift.[157]

In order to draw conclusions from the cell parameters assuming that they behave as viscoelastic bodies, an impedance analysis in the range of the resonance frequencies of the quartz is necessary. Complex shear moduli can be obtained by fitting electromechanical models to the obtained data. In Figure 25 the impedance behavior of a 5 MHz quartz in the presence and absence of adherent Madin darbine canine kidney (MDCK II) cells is shown. The quartz is highly damped because of the attached cells—an indication that they do not behave like a rigid mass. Modeling the cells attached to the resonator as a Newtonian liquid turns out to be too simplified to account for its impedance behavior on the resonator. In fact it is apparent from the spectra that an elastic contribution has to be considered.[158] A detailed analysis of the individual components of an adherent cell monolayer on a quartz plate illuminates the complexity of the system. Besides

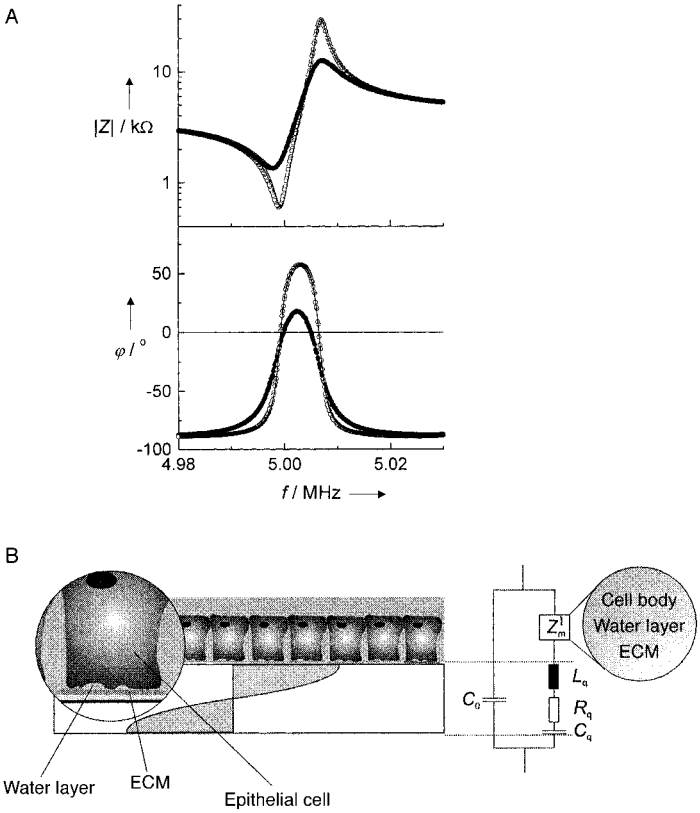

Figure 25. A) Influence of a confluent MDCK II cell monolayer on the impedance spectrum of a 5 MHz quartz resonator ($|Z|$ and φ); the spectra before (●) and after (○) scraping the cell layer from the surface are shown. The solid lines are the results of curve fitting using the BVD-equivalent circuit. B) Equivalent circuit of an adherent cell monolayer including extracellular matrix (ECM) and water layer. Z_m^1 represents the combined viscoelastic properties of adherent cells as well as the ECM and an adjacent water layer between the cell and the surface.[167]

the actual cell layer, the extracellular matrix (ECM), a water film between the ECM and cell, and the medium on top of the cells need to be considered. It was shown that the influence of the extracellular matrix plays a pivotal role in the shear oscillation, while the mechanical properties of a cell-covered quartz resonator remain unaffected by the supernatant medium. The contribution of the ECM is mainly inductive and can therefore be considered as a simple mass added to the

resonator. Energy dissipation, however, could not be observed.[159]

Damping of the shear oscillation by the presence of a confluent cell monolayer is dependent on the particular cell species and their ability to adhere on the surface. Loosely attached bovine aortic cells have little effect on the motional resistance R, while strongly adhered MDCK cells damp the oscillation of the quartz considerably (Table 6). This difference can be explained by the presence of a variable, thin water layer between the cell and the surface. Diminishing the thickness of the water layer by applying hyperosmotic stress, in which the osmolyte does not penetrate the cell layer (saccharose), leads to a dramatically increased damping of the shear oscillation (Figure 26).

Table 6. Change of the motional resistance R and inductance L of different cell species. The parameters were obtained from the fitting of the BVD-equivalent circuit before and after mechanical removal of the confluent cell layer.[195]

Cell species	ΔR [Ω]	ΔL [μH]
MDCK I	755 ± 36	6.7 ± 0.7
MDCK II	992 ± 36	10.5 ± 0.8
Plexus epithelia	804 ± 43	16 ± 1.5
BAEC	55 ± 12	3.1 ± 0.5
3T3-fibroblasts	277 ± 20	2.5 ± 0.5

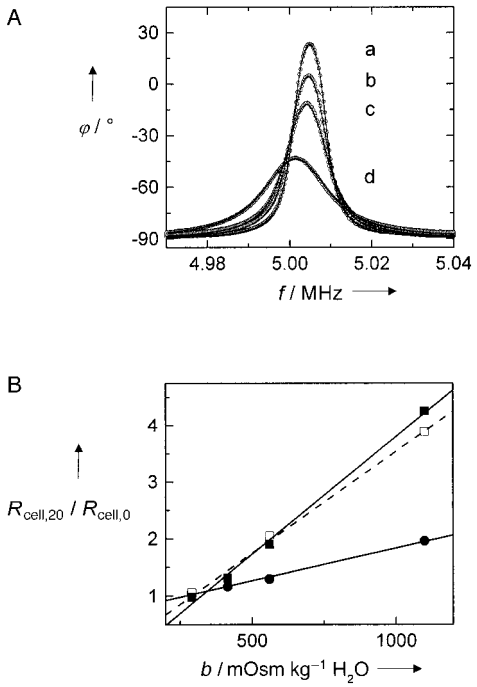

Figure 26. A) Phase spectra obtained from a quartz resonator covered with a confluent MDCK I cell layer upon sequential increase in the concentration of the osmotically active substances; a) 290, b) 415, c) 560, d) 1100 mOsm per Kg H_2O. The solid lines are the results of a fitting procedure using the BVD-equivalent circuit. B) Change of the relative motional resistance as a function of the molality of the osmotically active substances for MDCK I (□), MDCK II (■), and 3T3 cells (●). The motional resistance $R_{cell,20}$ was obtained 20 min after exchange of the isotonic medium for the indicated molality of the osmotically active substances, and is related to the initial resistance $R_{cell,0}$. The solid lines are the results of linear regressions.[159]

Wegener et al.[159] demonstrated that the observed increase in damping may probably not be attributed solely to a reduction of the cell volume;[160] instead, an osmotic-driven water flow out of the cell–substrate interspace presumably occurs, and this moves the cells more closely to the quartz surface and increases the damping.[161]

On the basis of the previous considerations, a quantitative analysis of the impedance data should ascribe a cell-covered quartz surface as a three layer model consisting of a rigid mass (ECM), a thin liquid layer between the ECM and cell body, and a semi-infinite viscoelastic body, the cell. A detailed analysis of this multicomponent system is the subject of current investigations.

Besides from data of confluent cell monolayers obtained under static conditions, time-resolved processes, such as cell adhesion or the influence of pharmacological substances, can also be monitored using the quartz-crystal microbalance in the active or passive mode. The process of cell adhesion is rather complex and characterized by several distinct processes which influence the oscillation behavior of the quartz resonator. Starting with the first physical contact of the cell with the surface, processes such as cell spreading, that is, the enlargement of the contact area of the cell with the surface, modification of the adhesion properties, excretion of extracellular matrix components, and changes of the cell's cytoskeleton influence the oscillation in various ways. A detailed study of cell adhesion based on a time-resolved frequency analysis was performed by Wegener et al.[162] using different cell lines (MDCK I and II cells as well as 3T3-fibroblasts). Wegener et al. confirmed the presumptions of Redepenning et al.[155] and Matsuda et al.[163] that the frequency decrease is correlated with the number of cell–substrate contacts. Cells that do not form contacts with the surface as a result of the presence of contact-inhibiting peptides (RGD sequences) or cell death that prevent adhesion, do not change the resonance frequency of the quartz (Figure 27).

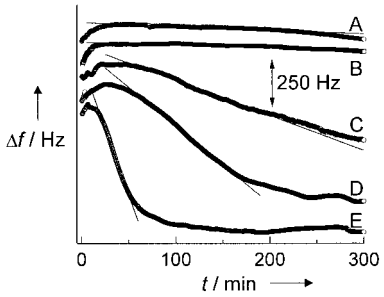

Figure 27. Time course of the resonance frequency during the adhesion of MDCK II cells starting with seeding densities of $(8 \pm 1) \times 10^5$ cm^{-2} in the presence of A) 1 mM GRGDS; B) 1 mM RGDS; C) 2 mM RGD; D) 1 mM RGD, and E) 1 mM SDGRG. The solid lines are linear regressions to enable the apparent adhesion rates to be determined.[162]

If a comprehensive impedance analysis of the quartz oscillation is not possible, or a higher time-resolution than provided by impedance analysis is required, changes in the dissipation factor $D = Q^{-1}$ of the oscillation, which represents the energy dissipation upon the binding of cells to the resonator surface, can be monitored. In this way Kasemo and

co-workers were able to detect the adsorption of monkey kidney epithelial (MKE), Chinese hamster ovary (CHO) cells, and neutrophiles by measuring the frequency shift of the quartz and the time-resolved energy dissipation simultaneously.[164, 165] Otto et al.[166] used the same technique to investigate the interaction of *E. coli* with surfaces varying in their hydropathic behavior. These experiments showed that contact area, surface energy, ionic strength, and the cell surface influence the frequency and dissipation changes considerably.

If cell monolayers exhibit interesting barrier-forming properties as a consequence of the presence of tight junctions, the quartz-crystal microbalance can be combined with common electrochemical techniques. Such a setup allows the performance of a so-called quasi-simultaneous double-mode impedance analysis, as described by Janshoff et al.[167] (Figure 28).

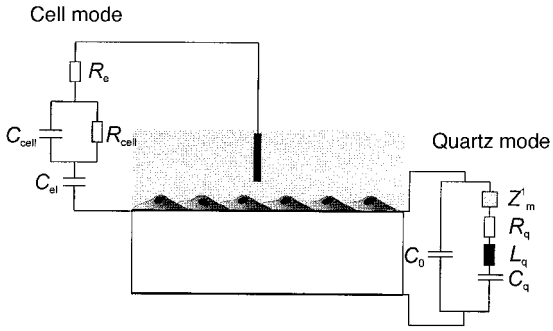

Figure 28. Schematic drawing of cells that are adhered to a quartz plate and the corresponding equivalent circuits used for the impedance spectra obtained in quartz mode and cell mode.[167]

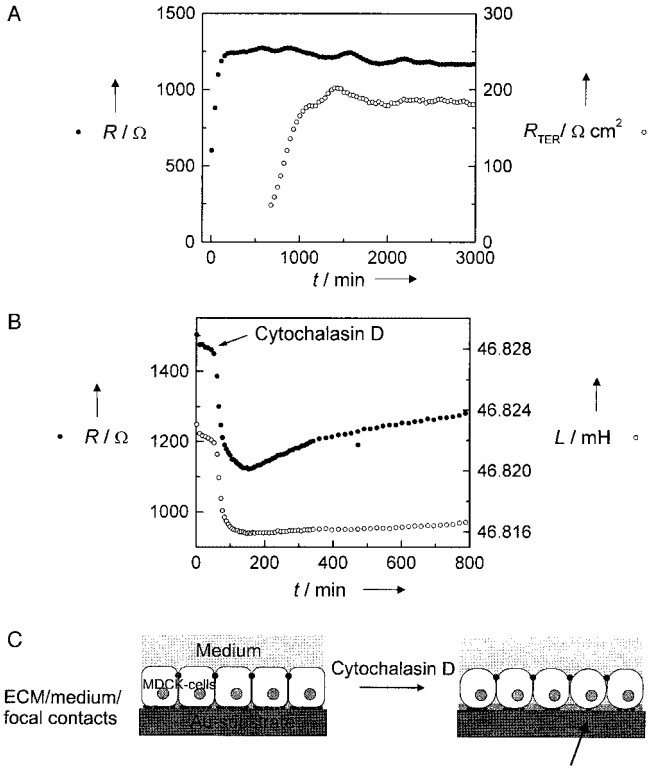

Figure 29. A) Time course of the motional resistance R (●) and transepithelial resistance R_{TER} (○) when a confluent MDCK II cell layer is formed on a 5 MHz quartz. The seeding density was $(1.5 \pm 0.2) \times 10^6$ cells per cm^2. B) Time course of the motional resistance R (●) and the induction L (○) of a MDCK II-covered 5 MHz quartz upon addition of the alkaloid cytochalasin D with a concentration of 5 μm. C) Conceivable scenario of the influence of cytochalasin D on a confluent cell layer. The arrow indicates the decreased contact area of the cells with the surface as a result of the rounding of the cell bodies.[109]

With this setup it is possible to detect electrical and viscoelastic properties of cell monolayers with one device. A cell monolayer can be described by a parallel *RC* element in series with a capacitance C_{el}, which represents the electrode–solution interface; the corresponding equivalent circuit is depicted in Figure 28. Figure 29A shows the time course of the transepithelial and motional resistance after the seeding of MDCK II cells on a quartz resonator. Damping of the shear oscillation occurs immediately after seeding, whereas the transepithelial resistance can only be detected after 15 h. The adhesion of cells, which predominately determines the damping behavior of the cells, occurs long before the formation of tight junctions. Morphological changes of the cells induced by changes of the cytoskeleton can be monitored time-resolved with this device, as demonstrated by the example of cytochalasin D (alkaloid), which inhibits the polymerization of actin filaments (Figure 29B, C). The induced rounding of the cells by the degradation of the actin filaments results in a decreased contact area of the cells with the resonator and an increase in the average distance of the cells to the substrate; as a consequence a decrease in the characteristic damping of the shear oscillation by a confluent cell monolayer occurs. Moreover, it was shown that the transepithelial resistance collapses as a result of the large morphological changes.

3.7. Functionalized Vesicles as Model Systems for Cell Adhesion

As a consequence of the complexity of the cell and its contacts to the surface, it is quite difficult to address the question as to which properties of the cell mostly influence the resonance frequency shift. A simplified system to model the surface adhesion of cells in detail are receptor-doped lipid vesicles, which can interact with surface-confined ligands.[168] Pignataro et al.[169] scrutinized the interaction of biotinylated lipid vesicles with a streptavidin and avidin matrix. It turned out that the frequency decrease of the quartz was determined by the extent of biotinylation within the vesicles (Figure 30).

However, the frequency decrease could not solely be explained with the number of adsorbed vesicles on the surface. A complementary scanning force microscopy study demonstrated that an increase in the degree of biotinylation of the vesicles, that is, an increased number of biotin–streptavidin bonds, leads to a more pronounced flattening of the vesicles up to a biotin content where the vesicles disrupt and start to spread on the surface and form planar lipid bilayers. The authors drew the conclusion that the number of contacts influences the frequency response of the quartz. The connection between the contact area and frequency decrease was

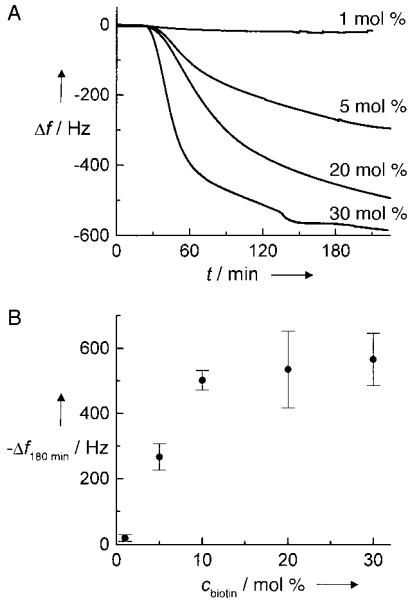

Figure 30. A) Frequency decrease of a 5 MHz quartz upon binding of vesicles doped with different amounts of biotin-X-DHPE to an avidin layer. B) Frequency shift 180 min after addition of vesicles.[169]

also observed by Liebau et al.[170, 171] They demonstrated that polymerized liposomes produce a significantly smaller frequency decrease than nonpolymerized ones. They explained this observation through a suppressed membrane fusion. As already demonstrated by Ohlson et al.[172] and Janshoff et al.[107] fusion of vesicles on the surface results in large frequency shifts of more than 230 Hz using a 5 MHz quartz. Presumably, a significant change in the surface energy might be responsible for the observed frequency shift.[173] A more detailed explanation remains to be elucidated.

4. Development of Biosensors Based on Optical Transducers

In this section the acoustic resonators described above are compared with common state of the art optical transducers as used for bioanalytic purposes. In principle, information about the quantity of an analyte can be obtained from the characteristic properties of light, such as frequency, amplitude, phase, or polarization. In the area of biosensor development several label-free optical methods, such as surface plasmon resonance spectroscopy (SPR),[174–176] grating coupler, reflectance interference spectroscopy (RIfS),[177] and ellipsometry have been established.[178] These techniques all detect the refractive index n and the film thickness d or the effective optical thickness (nd). The general principles of different optical techniques are depicted in Figure 31.

The specificity of those sensors is achieved by surface-immobilized receptive layers. The process of functionalization has to be adapted to the properties of the sensor surface. Thus, thiol chemistry is suitable for SPR and ellipsometry while silane chemistry is advantageous for glass surfaces (grating coupler, interferometry). In the following sections different techniques with significant commercial impact, such as SPR,

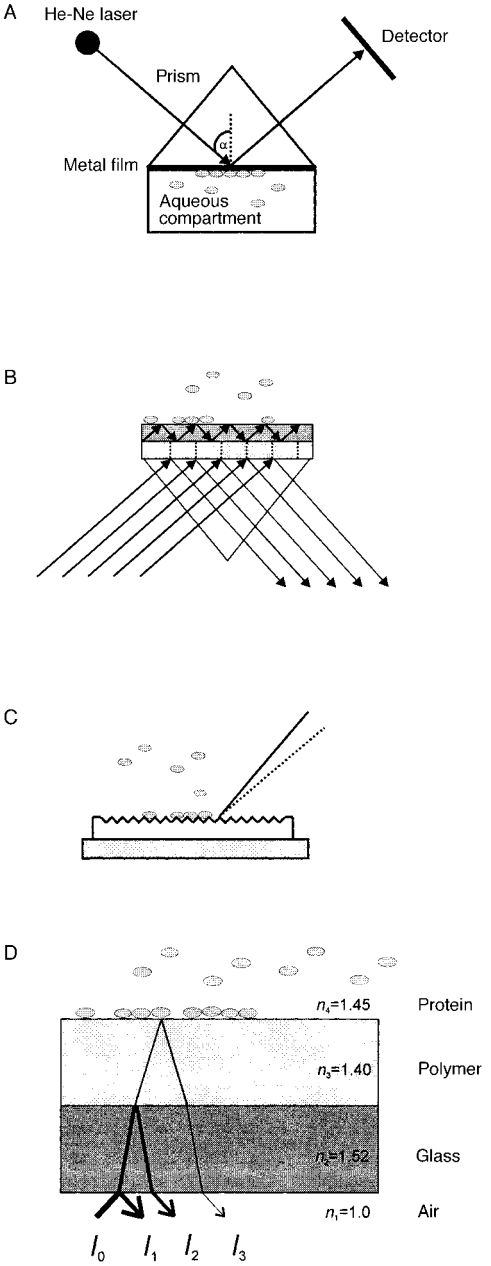

Figure 31. Schematic representation of the device principles of different optical label-free techniques. A) Surface plasmon resonance spectroscopy (SPR); B) resonance mirror (RM); C) grating coupler, and d) reflectometric interferometric spectroscopy (RIfS).

grating couplers, the resonance mirror technique, and interferometry (RIfS), are explained in more detail and different parameters, such as sensitivity, detection range, and their limitations, are discussed and compared to acoustic resonators.

4.1. Grating Coupler and Resonance Mirror Technique

Evanescent field techniques are based on multiple reflections at the interface between a substrate and a thin film ($d <$ 1 μm) immobilized on a surface composed of biological receptive layers that show a lower refractive index than the

supporting substrate. The detection limit is considerably lowered when the system is equipped with an optical waveguide with multiple reflections since the relative propagation velocity of the guided wave depends not only on the refractive index of the medium but also on the number of reflections. Guidance of the wave is accomplished by an imprinted grating structure on the surface using a certain angle of incidence. Observing the intensity after the wave has traveled through the material at the end of the film is the easiest way of measurement.[177]

However, in most cases this technique is used as a differential interferometer in which the different propagation velocities of the waves for different polarizations are considered. As *E*- and *B*-field vectors of the electromagnetic radiation are orthogonal, they will propagate with different velocity, dependent on the refractive index of the surface confined compound. The detectable phase difference, or strictly speaking its change, is a measure of the altered refractive index, for example, on the binding of an analyte to a receptive surface.

The resonance mirror (RM) technique[177] is based on a prism coupler; the coupling conditions for two orthogonal waves of linear polarized light are met at different angles of incidence. The polarized waves experience a phase shift in the waveguide. Linear polarized light with an incident angle of 45° is used in a typical experiment. The observed ellipticity after travelling through the waveguide depends not only on the phase shift, and therefore considerably on the refractive index, but also on the adsorption layer at the interface. Thus, the ellipticity is again a direct measure of the amount of surface-bound analytes. The main applications of both methods in the field of biosensors are the detection of antigen – antibody reactions.

4.2. Surface Plasmon Resonance

Surface plasmon resonance spectroscopy (SPR) utilizes the evanescent field in the same fashion as the resonance mirror technique for the determination of the refractive index close to the sensor surface. Surface plasmons are longitudinal electron-density oscillations at the interface of a metal and a dielectric medium, for example. Surface plasmon resonance occurs by optical excitation only if the wave of the incoming light interacts with the free electrons of the metal and if the energy and momentum of the incident light beam correspond to those of the surface plasmons. The dispersion relation between frequency ω and wave number k of the plasmons at the interface [Eq. (18) ε_m and ε_d are the dielectric constants of the metal film and the dielectric medium, respectively] is decisive for excitation.

$$k = \frac{\omega}{c}\sqrt{\frac{\varepsilon_d \varepsilon_m}{\varepsilon_d + \varepsilon_m}} \tag{18}$$

Excitation is accomplished by attenuated total reflection, with the compound under investigation being immobilized on a glass prism covered with an evaporated metal film. In this setup, plasmons are excited by an evanescent electromagnetic field which induces oscillation of the free electrons in the metal. Only p-polarized light is capable of exciting surface plasmons. However, these plasmons generate another electromagnetic field, which penetrates the dielectric medium closely attached to the metal surface. Only at a certain angle of incidence do the wave numbers of radiation and surface plasmons match, which leads to a resonance phenomenon in which the energy of photons is transferred to plasmons. Plasmon resonance can be observed as a sharp minimum in the reflectivity of the incident light beam. The angle of incidence of monochromatic light is varied during an experiment, and the reflectivity near the resonance monitored. As the wavelength is constant, the angle of the resonance minimum only depends on the dielectric constant of the medium covering the metal layer and is thus a measure of the concentration of an analyte adsorbed on the functionalized metal surface.

SPR can be used as a spectroscopic as well as a microscopic technique, which leads to an increasing number of applications of this optical method. Thus, SPR is used not only for studying classical ligand – receptor interactions in biochemistry but also for the detection of binding events at lipid membranes, similar to the quartz crystal microbalance technique. Special methods are required to modify these surfaces, which are essentially based on the fusion of liposomes onto hydrophobic surfaces. The interested reader is referred to the review articles of Salamon et al.[175, 176] The high sensitivity at a distance up to 100 nm away from the gold surface allows the imaging of focal contacts of adherent cells by SPR microscopy.[180]

4.3. Reflectometric Interference Spectroscopy

While both label-free methods discussed above detect changes in the refractive index upon analyte binding using an evanescent field, the reflectometric interference spectroscopy directly determines the effective thickness and thus the surface concentration of the analyte. This bound analyte layer exhibits a thickness of up to 10 nm in the case of biomolecules, but only 0.1 nm for low molecular weight compounds.[177] The physical principle of this method is a wavelength modulation of the reflectivity of a thin transparent film (Figure 31 D). When a film is illuminated with white light through a substrate it is reflected at both interfaces of the film. If monochromatic light is used, either constructive or destructive interference is observed, dependent on the phase shift; the interference obtained using white light varies upon the wavelength, so that a periodic modulation of the reflecting light intensity—an interference spectrum—results. Thus, the positions of the maxima and minima only depend on the film thickness at a given refractive index and angle of incidence. The constructive interference obtained by illumination along an axis coincident with the surface normal is given by Equation (19), in which m is the order of the maxima.

$$2nd = m\lambda \tag{19}$$

An increase in the thickness of the transparent layer results in a shift of the spectrum to larger wavelengths and is strictly valid only for transparent films with a thickness in the range of

the wavelength of the incoming light. This is not true for high molecular weight biomolecules and low molecular weight analytes. Nevertheless, a simple experimental trick enables one to obtain defined interference spectra, for example, a glass substrate is covered with a thick interference layer of a polymer material such as gels or oxides (SiO_2). This layer, which exhibits an interference pattern, is then functionalized by receptor molecules. As a consequence, a change in the thickness because of the adsorption of the complementary binding partner can be measured. The thickness change is far below the wavelength of radiation. This method allows measurements of thickness changes down to 1 pm resolution in effective optical thickness. Gauglitz and co-workers used this technique to quantify antigen–antibody reactions as an example of high molecular weight analytes as well as the binding of pesticides (triazine) as an example for low molecular weight analytes. They immobilized anti-pesticide antibodies on an interference layer and determined the thickness change, which was partially below 1 pm.

In special cases porous surfaces obtained from *p*-type silicon are used as an alternative to polymer films.[181] These thin meso- to macroporous films serve not only for the generation of interference maxima and minima but also provide a signal enhancement arising from the large increase in the surface area within the porous matrix. The inner cavities of the pores need to be properly functionalized, which is achieved either by using trialkoxysilanes or Lewis acids and Grignard reagents to generate Si–C bonds.[182–184] Reflectometry as well as the other optical methods can be applied to all kinds of binding problems and is an attractive alternative to common ELISA techniques, although it is less sensitive. Furthermore, reflectometry is suited to deal with thermodynamic and kinetic problems. Optical transducers as used in reflectometry reveal a high potential for detecting pharmaceutically relevant analytes.

5. Comparison of the Application of the QCM with Optical Methods

A detailed comparison of the QCM and SPR method was published in 1995 by Kößlinger et al.[185] In this work a QCM and SPR spectrometer were realized in one setup. The authors claimed that no significant difference between both techniques could be notified in terms of sensitivity and cross reactivity. Both measurement devices are equally suited for the online detection of chemical and biological analytes and work without chemical modifications of the analyte. The essentially different measurement principles (mass density for QCM and dielectric constant for SPR), however, lead inevitably to different limitations with respect to sensitivity, signal to noise ratio, accuracy, reproducibility, regeneration of the sensor surface, suitability for different complex analyte systems, handling, and cost.

For SPR transducers, the metal film is evaporated on glass substrates, which are transparent for lasers in the visible region, or silicon chips, which are transparent in the IR region.[174] Optical components such as simple glass fibers, ATR-prism couplers, grating couplers, or integrated layer systems can be used as optical waveguides. The cost of such a setup is about two times higher than that of a QCM, which comprises a frequency counter, voltage supply, and an oscillator circuit. Table 7 summarizes typical properties of the different measuring devices.

The comparison of Kößlinger et al.[185] basically demonstrates that both techniques are equally suited for bioanalytics. Affinity measurements can be satisfactorily performed with both devices (Figure 32).

The great advantage of SPR over QCM is its small sensor area (5×10^{-3} mm^2 in comparison to 5 mm^2 for QCM) and the higher sensitivity, namely, a greater number of particles is detectable on the effective sensor surface (10^{-17} mol for SPR and 10^{-14} mol for QCM). The quartz-crystal microbalance is, however, more suited for the determination of material properties such as the viscoelasticity of polymer films.

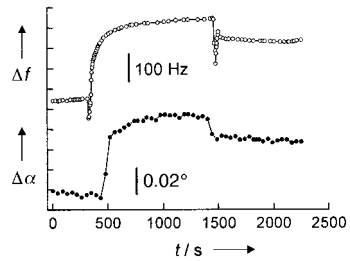

Figure 32. Change in the resonance frequency (○) and SPR angle (●) upon nonspecific adsorption of bovine serum albumin to a gold surface.[185]

Table 7. Comparison of surface plasmon resonance spectroscopy (SPR) with the quartz-crystal microbalance (QCM; 20 MHz quartz) on the basis of their special properties.[185]

	QCM	SPR
wave equation	Christoffel equation	Maxwell equation
wave type	elastic shear waves	surface plasmons
basic physical quantities	mechanical impedance $\boldsymbol{Z}$	reflectivity
measuring quantities	frequency, quality factor, impedance	angle of reflectivity minimum
material parameter	film thickness, density, viscosity, surface tension, viscoelasticity, ionic strength	dielectric constant, film thickness
penetration depth in water	126 nm	150 nm ($\lambda = 1300$ nm)
influence of ionic strength	can be neglected	large
sensitive area	5 mm^2	0.005 mm^2
detection limit	10^{-14} mol	10^{-17} mol
thickness sensitivity/protein film	184 Hz nm^{-1}	0.0263° nm^{-1}
minimal significant change of the measuring quantity	20–25 Hz	0.005°
minimal detectable mass	30 ng per 5 mm^2	0.5–5 ng per 5×10^{-3} mm^2
sensitivity calibration	electrolysis	–

6. Summary and Outlook

In the last few years the quartz-crystal microbalance has developed from a pure mass sensor in the gas phase into a versatile tool in chemo- and bioanalytics which not only provides information about binding events at surfaces, but also reveals material-specific quantities, such as elasticity moduli, surface charge densities, and viscosity. Indirectly, one can also deduce conformational changes of proteins as well as the water content and net charge of biomolecules from the data. Potential applications are quantification of cell adhesion and the determination of viscoelastic properties of adherent cells. It is expected that TSM resonators will become to be a real alternative to conventional cell-specific techniques, such as cell counting and optical microscopy, to control cell culture. Many active substances directly influence cell adhesion. Hence, the quartz-crystal microbalance is a fast and sensitive device providing information about cell–substrate interactions, the alteration of the number of focal contacts, or the distance of the cell from the substrate. Moreover, the possibility of combining the quartz-crystal microbalance with other techniques, for example, optical (SPR) or electromechanical techniques (EQCM), will increase the knowledge about processes at interfaces in biochemistry as they occur at cell surfaces. In this way double mode impedance analysis allowed alterations of the barrier properties and cell substrate interactions of cell monolayers to be correlated in a time-resolved fashion and quasi-simultaneously. While the electrochemical QCM is already routinely used in electrochemistry for monitoring deposition and corrosion processes, a combination of voltammetry, chronoamperometry, and impedance analysis with QCM is rarely used in bioanalytics.

In summary, the detection limit of the quartz-crystal microbalance is poorer than that of optical methods such as SPR or RIfS, which is partially a result of the larger sensor surface area, and partially a result of the inherent sensitivity. In most cases, a lower sensitivity does not hinder the investigation of biological problems since equilibrium thermodynamic and kinetic data cannot be obtained beyond picomolar concentrations as a consequence of the limited volume. A continuous depletion in solution would result—this is also true for surface plasmon resonance spectroscopy, though SPR spectroscopy needs a considerably smaller detection area, since the sensor area covered with adsorbed molecules is in general larger than the detected one. As far as the QCM is concerned miniaturization is naturally limited, which plays an important role with respect to the desired automation because of the need for small reaction chambers. The power of piezoelectric sensors is definitely the vast quantity of available information that can be obtained and the reliable determination of thermodynamic and kinetic data. The method allows the use of almost any material from metals to dielectric surfaces. In order to achieve lower detection limits for minor component analysis it is necessary to use piezoelectric sensors with higher mass sensitivity, such as APM and FPW sensors, though these methods need to be further developed.

Received: 21 December, 1999 [A 378]

[1] R. Schumacher, *Angew. Chem.* **1990**, *102*, 347; *Angew. Chem. Int. Ed. Engl.* **1990**, *29*, 329.
[2] D. A. Buttry, M. D. Ward, *Chem. Rev.* **1992**, *92*, 1355.
[3] G. Sauerbrey, *Z. Phys.* **1959**, *155*, 206.
[4] T. Nomura, M. Okuhara, *Anal. Chem.* **1982**, 281.
[5] B. A. Martin, H. E. Hager, *J. Appl. Phys.* **1989**, *65*, 2630.
[6] J. F. Rosenbaum, *Bulk Acoustic Wave Theory and Devices*, Artechhouse, Boston, **1988**.
[7] D. S. Ballantine, R. M. White, S. J. Martin, A. J. Ricco, E. T. Zellers, G. C. Freye, H. Wohltjen, *Acoustic Wave Sensors*, Academic press, San Diego, **1997**.
[8] G. Kurz, W. Mathis, *Oszillatoren*, Hüthig, Heidelberg, **1994**.
[9] a) V. E. Bottom, *Introduction to Quartz Crystal Unit Design*, van Nostrand Reinhold, New York, **1982**; b) $v_p = \sqrt{c/\rho}$.
[10] T. A. Jones, M. Kleitz, I. Lundström, W. Göpel, *Micro- and Nanosensor Technology/Trends in Sensor Markets*, VCH, Weinheim, **1995**.
[11] c_{66} is the piezoelectric stiffened elastic modulus of the quartz crystal obtained from the coupling of the mechanical displacement with the potential in planar piezoelectric waves: $c_{66} = c_{66} + e_{26}^2/\varepsilon_{22}$.
[12] a) A. C. Hillier, M. D. Ward, *Anal. Chem.* **1992**, *64*, 2539; b) the solution to the wave equation assumes the following boundary conditions: $\mathbf{u}(r,\theta,z,t) = \Sigma A_{mn} J_m(\lambda_{mk}\frac{r}{R})(C_m\cos(m\theta) + D_m\sin(m\theta)) \cdot \sin\left(\frac{n\pi}{d_q}z\right)\sin(\omega_{mnk}t)$, with $m = 0,1,2 \ldots$, $n = 1,3,5 \ldots$, $k = 1,2,3 \ldots$, and the constants A_{mn}, C_m, and D_m of the shear oscillation, which depend on the initial conditions. J_m is the Bessel function of first kind and order m, λ_{mk} are the positive roots of the Bessel function.
[13] In addition, in the case of small resonators with large thickness, the resonance frequency depends considerably on the lateral dimensions of the circular-shaped plate as apparent from the second term.
[14] An AT-cut quartz crystal exhibits thickness excitation (TE) and lateral field excitation (LFE); the first one generates transversal the last one longitudinal waves.
[15] Notably, Equation (2) describes basically the serial resonance ($Z \rightarrow 0$). The difference between the antiresonance ($Z \rightarrow \infty$) and serial resonance is manifested in the electroacoustic constant k_t: $\omega_a^2 - \omega_s^2 = 8k_t(\bar{c}_{66}/\rho_q d_q^2)$.
[16] W. P. Mason, *Physical Acoustics*, *Vol. 2A*, Academic Press, New York, **1965**.
[17] S. J. Martin, V. E. Granstaff, G. C. Frye, *Anal. Chem.* **1991**, *63*, 2272.
[18] M. Yang, M. Thompson, *Anal. Chem.* **1993**, *65*, 1158.
[19] A. L. Kipling, M. Thompson, *Anal. Chem.* **1990**, *62*, 1514.
[20] A decrease in the resonator dimension results also in the reduction of the spurious modes since the resonance frequencies become separated. In particular, spurious modes occur if the thickness of the electrodes is too small.
[21] As a result of the nonpiezoelectric electrode mass the electroacoustic coupling constant decreases, which leads to a stronger convergence of the resonance frequencies (anti- and serial resonance). This allows the resonator to be tuned over a wide frequency range.
[22] F. Josse, Y. Lee, S. J. Martin, R. W. Cernosek, *Anal. Chem.* **1998**, *70*, 237.
[23] B. A. Martin, H. E. Hager, *J. Appl. Phys.* **1989**, *65*, 2627.
[24] C. E. Reed, K. K. Kanazawa, J. H. Kaufman, *J. Appl. Phys.* **1990**, *68*, 1993.
[25] H. L. Bandey, S. J. Martin, R. Cernosek, *Anal. Chem.* **1999**, *71*, 2205.
[26] V. E. Granstaff, S. J. Martin, *J. Appl. Phys.* **1994**, *75*, 1319.
[27] E. Benes, *J. Appl. Phys.* **1984**, *56*, 608.
[28] C. Lu, D. Lewis, *J. Appl. Phys.* **1972**, *43*, 4385.
[29] K. K. Kanazawa, J. G. Gordon, *Anal. Chem.* **1985**, *57*, 1770.
[30] E. Nwankwo, C. J. Durning, *Sens. Actuators A* **1999**, *72*, 99.
[31] E. Nwankwo, C. J. Durning, *Sens. Actuators A* **1999**, *72*, 195.
[32] $h < 10$ μm, $G' > 10$ GPa.
[33] Z. Lin, M. D. Ward, *Anal. Chem.* **1995**, *67*, 685.
[34] W. T. Schneider, S. J. Martin, *Anal. Chem.* **1995**, *67*, 3324.
[35] An alteration of the ion conductivity and dielectric constant affects the length of the electrochemical double layer, which in turn influences the resonance frequency of the quartz resonator. Changes in the density and viscosity of the water layer near the resonator's surface, together with real mass changes, also play a considerable role. This effect is, however, small compared to the frequency shifts

of the parallel resonance arising from the contribution of ionic conductivity in solution.
[36] The serial resonance is determined by the mechanical properties of the quartz, while the parallel resonance is determined by the mechanical *and* electric properties.
[37] Z. Shana, F. Josse, *Anal. Chem.* **1994**, *66*, 1955.
[38] M. Rodahl, F. Höök, B. Kasemo, *Anal. Chem.* **1996**, *68*, 2219.
[39] Kasemo and co-workers found that the dissipation factor shows a maximum while the parallel resonance frequency reaches a minimum value at high frequencies. Dependent on the electrode form, frequency shifts of more than 1000 Hz can be observed for a 5 MHz quartz upon changing the solution ($0 \rightarrow 1\ S\,m^{-1}$).
[40] R. Beck, U. Pittermann, K. G. Weil, *J. Electrochem. Soc.* **1992**, *139*, 453.
[41] S. J. Martin, G. C. Frye, A. J. Ricco, *Anal. Chem.* **1993**, *65*, 2910.
[42] V. Tsionsky, L. Daikhin, E. Gileadi, *J. Electrochem. Soc.* **1996**, *143*, 2240.
[43] E. Benes, M. Gröschl, W. Burger, M. Schmid, *Sens. Actuators A* **1995**, *48*, 1.
[44] J. C. Andle, J. F. Vetelino, M. W. Lade, D. J. McAllister, *Sens. Actuators B* **1992**, *8*, 192.
[45] S. J. Martin, A. J. Ricco, T. M. Niemczyk, G. C. Freye, *Sens. Actuators* **1989**, *20*, 253.
[46] H. Lamb, *Proc. Roy. Soc. (London) Ser. A* **1917**, *93*, 114.
[47] B. A. Auld, *Acoustic Fields and Waves in Solids*, Wiley, New York, **1973**
[48] $B = \left(\frac{\lambda}{2\pi}\right)^{-2} \frac{E d^3}{12\,(1-\nu_P^2)}$ with the Young modulus E and the Poisson number ν_P.
[49] Z. Lin, C. M. Yip, I. S. Joseph, M. D. Ward, *Anal. Chem*. **1993**, *65*, 1546.
[50] S. Bruckenstein, M. Shay, *Electrochim. Acta* **1985**, *30*, 1295.
[51] C. Barnes, *Sens. Actuators A* **1991**, *29*, 59.
[52] M. Rodahl, F. Höök, A. Krpzer, P. Brzezinski, B. Kasemo, *Rev. Sci. Instrum.* **1995**, *66*, 3924.
[53] C. Zhang, G. Feng, *Ultrason. Symp. Proc.* **1996**, *43*, 942.
[54] N. C. Fawcett, J. A. Evans, L.-C. Chen, N. Flowers, *Anal. Lett.* **1988**, *21*, 1099.
[55] H. A. Su, Ph.D. thesis, University of Toronto, **1991**.
[56] Y. Okahata, M. Kawase, K. Niikura, F. Ohtake, H. Furusawa, Y. Ebara, *Anal. Chem.* **1998**, *70*, 1288.
[57] Y. Okahata, Y. Matsunobu, K. Ijiro, M. Mukae, A. Murakami, K. Makino, *J. Am. Chem. Soc.* **1992**, *114*, 8299.
[58] T. Sato, T. Kawakami, N. Shirakawa, Y. Okahata, *Bull. Chem. Soc. Jpn.* **1995**, *68*, 2709.
[59] K. Ito, K. Hashimoto, Y. Ishimori, *Anal. Chim. Acta* **1996**, *327*, 29.
[60] A. Bardea, A. Dagan, I. Ben-Dov, B. Amit, I. Willner, *Chem. Commun.* **1998**, 839.
[61] J. Wang, P. E. Nielsen, M. Jiang, X. Cai, J. R. Fernandes, D. H. Grant, M. Ozsoz, A. Beglieter, M. Mowat, *Anal. Chem.* **1997**, *69*, 5200.
[62] F. Caruso, E. Rodda, D. N. Furlong, V. Haring, *Sens. Actuators B* **1997**, *41*, 189.
[63] F. Caruso, E. Rodda, D. N. Furlong, K. Niikura, Y. Okahata, *Anal. Chem.* **1997**, *69*, 2043.
[64] R. C. Ebersole, J. A. Miller, J. R. Moran, M. D. Ward, *J. Am. Chem. Soc.* **1990**, *112*, 3239.
[65] F. Caruso, D. N. Furlong, K. Niikura, Y. Okahata, *Colloids Surf. B* **1998**, *10*, 199.
[66] Y. Okahata, K. Niikura, Y. Sugiura, M. Sawada, T. Morii, *Biochemistry* **1998**, *37*, 5666.
[67] H. Su, K. M. R. Kallury, M. Thompson, *Anal. Chem.* **1994**, *66*, 769.
[68] N. C. Fawcett, R. D. Craven, P. Zhang, J. A. Evans, *Anal. Chem.* **1998**, *70*, 2876.
[69] J. Wang, M. Jiang, T. W. Nilsen, R. C. Getts, *J. Am. Chem. Soc.* **1998**, *120*, 8281.
[70] K. Niikura, H. Matsuno, Y. Okahata, *J. Am. Chem. Soc.* **1998**, *120*, 8537.
[71] A. Bardea, A. Dagan, I. Willner, *Anal. Chim. Acta* **1999**, *385*, 33.
[72] H. Su, M. Thompson, *Biosens. Biolelectron.* **1995**, *10*, 329.
[73] H. Su, S. Chong, M. Thompson, *Biosens. Bioelectron.* **1997**, *12*, 161.
[74] H. Su, S. Chong, M. Thompson, *Langmuir* **1996**, *12*, 2247.
[75] J. Wang, M. Jiang, E. Palecek, *Bioelectrochem. Bioenerg.* **1999**, *48*, 477.
[76] M. Muratsugu, F. Ohta, Y. Miya, T. Hosokawa, S. Kurosawa, N. Kamo, H. Ikeda, *Anal. Chem.* **1993**, *65*, 2933.
[77] F. Höök, M. Rodahl, P. Brzezinski, B. Kasemo, *Langmuir* **1998**, *14*, 729.
[78] F. Höök, M. Rodahl, B. Kasemo, P. Brzezinski, *Proc. Natl. Acad. Sci. USA* **1998**, *95*, 12271.
[79] F. Höök, M. Rodahl, P. Brzezinski, B. Kasemo, *J. Colloid Interface Sci.* **1998**, *208*, 63.
[80] J. Rickert, A. Brecht, W. Göpel, *Anal. Chem.* **1997**, *69*, 1441.
[81] K. Niikura, K. Nagata, Y. Okahata, *Chem. Lett.* **1996**, 863.
[82] K. Niikura, H. Matsuno, Y. Okahata, *Chem. Eur. J.* **1999**, *5*, 1609.
[83] K. Ijiro, H. Ringsdorf, E. Birch-Hirschfeld, S. Hoffmann, U. Schilken, M. Strube, *Langmuir* **1998**, *14*, 2796.
[84] M. Lion-Dagan, I. Ben-Dov, I. Willner, *Colloids Surf. B* **1997**, *8*, 251.
[85] M. Laatikainen, M. Lindstrom, *J. Colloid Interface Sci.* **1988**, *125*, 610.
[86] T. S. Berzina, L. Piras, V. I. Troitsky, *Thin Solid Films* **1998**, *327 – 329*, 621.
[87] J. Rickert, A. Brecht, W. Göpel, *Biosens. Bioelectron.* **1997**, *12*, 567.
[88] F. Caruso, K. Niikura, D. N. Furlong, Y. Okahata, *Langmuir* **1997**, *13*, 3427.
[89] Y. Lvov, K. Ariga, T. Kunitake, *Chem. Lett.* **1994**, 2323.
[90] Y. Lvov, K. Ariga, I. Ichinose, T. Kunitake, *J. Am. Chem. Soc.* **1995**, *117*, 6117.
[91] Y. Lvov, K. Ariga, I. Ichinose, T. Kunitake, *Langmuir* **1996**, *12*, 3038.
[92] Y. M. Lvov, Z. Lu, J. B. Schenkman, X. Zu, J. F. Rusling, *J. Am. Chem. Soc.* **1998**, *120*, 4073.
[93] J. Anzai, Y. Kobayashi, Y. Suzuki, H. Takeshita, Q. Chen, T. Osa, T. Hoshi, X. Du, *Sens. Actuators B* **1998**, *52*, 3.
[94] J. Anzai, H. Takeshita, Y. Kobayashi, T. Osa, T. Hoshi, *Anal. Chem.* **1998**, *70*, 811.
[95] E. Sackmann, *Science* **1996**, *271*, 43.
[96] C. Steinem, A. Janshoff, W.-P. Ulrich, M. Sieber, H.-J. Galla, *Biochim. Biophys. Acta* **1996**, *1279*, 169.
[97] T. Sato, T. Serizawa, Y. Okahata, *Biochim. Biophys. Acta.* **1996**, *1285*, 14.
[98] T. Sato, T. Serizawa, Y. Okahata, *Front. Biomed. Biotechnol.* **1996**, *3*, 145.
[99] T. Sato, T. Serizawa, F. Ohtake, M. Nakamura, T. Terabayashi, Y. Kawanishi, Y. Okahata, *Biochim. Biophys. Acta* **1998**, *12*, 82.
[100] Y. Okahata, Y. Ebara, T. Sato, *MRS Bull.* **1995**, *20*(6), 52.
[101] Y. Ebara, Y. Okahata, *Langmuir* **1993**, *9*, 574.
[102] "The influence of serum on the spreading of tumor cells on synthetic glycolipid films": T. Sato, M. Endo, Y. Okahata, *Adv. Biomater. Biomed. Eng. Drug Delivery Syst.* (Iketani Conf. Biomed. Polym.) **1996**, *5*, 273.
[103] C. Steinem, A. Janshoff, H.-J. Galla, *Chem. Phys. Lipids* **1998**, *95*, 95.
[104] H. Ebato, J. N. Herron, W. Müller, Y. Okahata, H. Ringsdorf, P. Suci, *Angew. Chem.* **1992**, *104*, 1064; *Angew. Chem. Int. Ed. Engl.* **1992**, *31*, 1087.
[105] T. Molin, P. Fredman, L. Svennerholm, *FEBS Lett.* **1986**, *205*, 51.
[106] M. J. Swamy, D. Gupta, S. K. Mahanta, A. Surolia, *Carbohydr. Res.* **1991**, *213*, 59.
[107] A. Janshoff, C. Steinem, M. Sieber, H.-J. Galla, *Eur. Biophys. J.* **1996**, *25*, 105.
[108] A. Janshoff, C. Steinem, M. Sieber, A. el Baya, M. A. Schmidt, H.-J. Galla, *Eur. Biophys. J.* **1997**, *26*, 261.
[109] C. Steinem, A. Janshoff, J. Wegener, W.-P. Ulrich, W. Willenbrink, M. Sieber, H.-J. Galla, *Biosens. Bioelectron.* **1997**, *12*, 787.
[110] J. S. Garvey, D. H. Campbell, N. E. Cremer, *Methods in Immonology: A Laboratory Text for Instruction and Research*, W. A. Benjamin, Reading, **1977**.
[111] E. Engvall, *Methods Enzymol.* **1980**, *70*, 419.
[112] A. Shons, F. Dorman, J. Najarian, *J. Biomed. Mater. Res.* **1972**, *6*, 565.
[113] P. H. Ngeh-Ngwainbi, S. S. Foley, G. G. Kuan, J. Guilbault, *J. Am. Chem. Soc.* **1986**, *108*, 5444.
[114] B. König, M. Grätzel, *Anal. Chem.* **1994**, *66*, 341.
[115] K. Nakanishi, H. Muguruma, I. Karube, *Anal. Chem.* **1996**, *68*, 1695.

[116] J. M. Abad, F. Pariente, L. Hernandez, E. Lorenzo, *Anal. Chim. Acta* **1998**, *368*, 183.
[117] J. E. Roederer, G. J. Bastiaans, *Anal. Chem.* **1983**, *55*, 2333.
[118] M. Thompson, C. L. Arthur, G. K. Dhaliwal, *Anal. Chem.* **1986**, *58*, 1206.
[119] H. Muramatsu, J. Dicks, E. Tamiya, I. Karube, *Anal. Chem.* **1987**, *59*, 2760.
[120] K. Davis, R. T. Leary, *Anal. Chem.* **1989**, *61*, 1227.
[121] A. Barraud, H. Perrot, V. Billard, C. Martelet, J. Therasse, *Biosens. Bioelectron.* **1993**, *8*, 39.
[122] R. M. Carter, J. J. Mekalanos, M. B. Jacobs, G. J. Lubrano, G. G. Guilbault, *J. Immunol. Methods* **1995**, *187*, 121.
[123] S. Drost, S. Hauck, E. Yacoub-George, H. Wolf, S. Koch, C. Kößlinger, B. Hillerich, K. Hieber, *Mater. Sci. Forum* **1998**, *287–288*, 521.
[124] F. Aberl, H. Wolf, C. Kößlinger, S. Drost, P. Woias, S. Koch, *Sens. Actuators B* **1994**, *18–19*, 271.
[125] F. Aberl, C. Kößlinger, H. Wolf, *Methods Mol. Med.* **1998**, *13*, 519.
[126] C. Kößlinger, S. Drost, F. Aberl, H. Wolf, *Fresenius J. Anal. Chem.* **1994**, *349*, 349.
[127] E. Uttenthaler, C. Kößlinger, S. Drost, *Biosens. Bioelectron.* **1998**, *13*, 1279.
[128] E. Uttenthaler, C. Kößlinger, S. Drost, *Anal. Chim. Acta* **1998**, *362*, 91.
[129] I. Ben-Dov, I. Willner, E. Zisman, *Anal. Chem.* **1997**, *69*, 3506.
[130] J. S. Bovenizer, M. B. Jacobs, C. K. O'Sullivan, G. G. Guilbault, *Anal. Lett.* **1998**, *31*, 1287.
[131] M. Minunni, M. Mascini, R. M. Carter, M. B. Jacobs, G. J. Lubrano, G. G. Guilbault, *Anal. Chim. Acta* **1996**, *325*, 169.
[132] I.-S. Park, N. Kim, *Biosens. Bioelectron.* **1998**, *13*, 1091.
[133] C. Steegborn, P. Skadal, *Biosens. Bioelectron.* **1997**, *12*, 19.
[134] R. Blonder, S. Levi, G. Tao, I. Ben-Dov, I. Willner, *J. Am. Chem. Soc.* **1997**, *119*, 10467.
[135] H. Ebato, C. A. Gentry, J. N. Herron, W. Müller, Y. Okahata, H. Ringsdorf, P. A. Suci, *Anal. Chem.* **1994**, *66*, 1683.
[136] P. Skladal, M. Minunni, M. Mascini, V. Kolar, M. Franek, *J. Immunol. Methods* **1994**, *176*, 117.
[137] M. Liu, Q. X. Li, G. A. Rechnitz, *Anal. Chim. Acta* **1999**, *387*, 29.
[138] S. Storri, T. Santoni, M. Minunni, M. Mascini, *Biosens. Bioelectron.* **1998**, *13*, 347.
[139] R. C. Ebersole, M. D. Ward, *J. Am. Chem. Soc.* **1988**, *110*, 8623.
[140] A. Sargent, O. A. Sadik, *Anal. Chim. Acta* **1998**, *376*, 125.
[141] N. J. Geddes, E. M. Paschinger, D. N. Furlong, Y. Ebara, Y. Okahata, K. A. Than, J. A. Edgar, *Sens. Actuators B* **1994**, *17*, 125.
[142] N. J. Geddes, E. M. Paschinger, D. N. Furlog, F. Caruso, C. L. Hoffmann, J. F. Rabolt, *Thin Solid Films* **1995**, *260*, 192.
[143] I. Vikholm, W. M. Albers, *Langmuir* **1998**, *14*, 3865.
[144] J. Rickert, T. Weiss, W. Göpel, *Sens. Actuators B* **1996**, *31*, 45.
[145] J. Rickert, T. Weiss, W. Kraas, G. Jung, W. Göpel, *Biosens. Bioelectron.* **1996**, *11*, 591.
[146] I. Vikholm, W. M. Albers, H. Valimaki, H. Helle, *Thin Solid Films* **1998**, *327–329*, 643.
[147] A. Näbauer, P. Berg, *Sens. Actuators B* **1990**, *1*, 508.
[148] N. Miura, H. Higobashi, *Sens. Actuators B* **1993**, *13–14*, 188.
[149] C. Zhang, G. Feng, Z. Gao, *Biosens. Bioelectron.* **1997**, *12*, 1219.
[150] I. Willner, R. Blonder, A. Dagan, *J. Am. Chem. Soc.* **1994**, *116*, 9365.
[151] I. Willner, B. Willner, *Bioelectrochem. Bioenerg.* **1997**, *42*, 43.
[152] R. Blonder, I. Ben-Dov, A. Dagan, I. Willner, E. Zisman, *Biosens. Bioelectron.* **1997**, *12*, 627.
[153] A. Hengerer, J. Decker, E. Prohaska, S. Hauck, C. Kößlinger, H. Wolf, *Biosens. Bioelectron.* **1999**, *14*, 139.
[154] D. M. Gryte, M. D. Ward, W. S. Hu, *Biotechnol. Prog.* **1993**, *9*, 105.
[155] J. Redepenning, T. K. Schlesinger, E. J. Mechalke, D. A. Puleo, R. Bizios, *Anal. Chem.* **1993**, *65*, 3378.
[156] Y. C. Fung, *Biomechanics*, Springer, New York, **1994**.
[157] The decay length within the cell depends on the cell's viscosity.
[158] However, estimating the viscosity of a MDCK I or II monolayer with $R \propto (\eta\rho)^{1/2}$ leads to a value of approximately 0.1 g(cm s)$^{-1}$ for a cell layer. This value seems to be very small compared to that determined by other methods such as the micropipette technique, though the frequency used is much higher and the displacement much smaller.
[159] J. Wegener, J. Seebach, A. Janshoff, H.-J. Galla, *Biophys. J.* **2000**, *78*, 2821.
[160] While the viscosity is increased only by a factor of two as a result of hyperosmotic stress, the motional resistance is increased by a factor of six instead of $\sqrt{2}$.
[161] As a consequence of the existence of tight junctions, the cell monolayer behaves like a semipermeable membrane capable of passing water through it.
[162] J. Wegener, A. Janshoff, H.-J. Galla, *Eur. Biophys. J.* **1998**, *28*, 26.
[163] T. Matsuda, A. Kishida, H. Ebato, Y. Okahata, *ASAIO J.* **1992**, *38*, M171.
[164] G. Nimeri, C. Fredriksson, H. Elwing, L. Liu, M. Rodahl, B. Kasemo, *Colloids Surf. B* **1998**, *11*, 255.
[165] C. Fredriksson, S. Kihlman, M. Rodahl, B. Kasemo, *Langmuir* **1998**, *14*, 248.
[166] K. Otto, H. Elwing, M. Hermansson, *J. Bacteriol.* **1999**, *181*, 5210.
[167] A. Janshoff, J. Wegener, M. Sieber, H.-J. Galla, *Eur. Biopys. J.* **1996**, *25*, 93.
[168] K. Yun, E. Kobatake, T. Haruyama, M. E. Laukkanen, K. Keinanen, M. Aizawa, *Anal. Chem.* **1998**, *70*, 260.
[169] B. Pignataro, C. Steinem, H.-J. Galla, H. Fuchs, A. Janshoff, *Biophys. J.* **2000**, *78*, 487.
[170] M. Liebau, G. Bendas, U. Rothe, R. H. H. Neubert, *Sens. Actuators B* **1998**, *47*, 239.
[171] M. Liebau, A. Hildebrand, G. Bendas, U. Rothe, R. H. H. Neubert, *Pharm. Ind.* **1999**, *61*, 459.
[172] P.-A. Ohlsson, T. Tjaernhage, E. Herbai, S. Loefas, G. Puu, *Bioelectrochem. Bioenerg.* **1995**, *38*, 137.
[173] J. Wang, L. M. Frostmann, M. D. Ward, *J. Phys. Chem.* **1992**, *96*, 5226.
[174] J. Homola, S. S. Yee, G. Gauglitz, *Sens. Actuators B* **1999**, *54*, 3.
[175] Z. Salamon, H. A. Macleod, G. Tollin, *Biochim. Biophys. Acta* **1997**, *1331*, 117.
[176] Z. Salamon, H. A. Macleod, G. Tollin, *Biochim. Biophys. Acta* **1997**, *1331*, 131.
[177] A. Brecht, G. Gauglitz, W. Nahm, *Analysis* **1992**, *20*, 135.
[178] J. A. De Feijter, J. Benjamins, F. A. Veer, *Biopolymers* **1978**, *17*, 1759.
[179] R. Kush, J. M. Cronin, W. J. Stuart, C. H. Maule, J. Molloy, N. J. Goddard, *Biosens. Biolelectron.* **1993**, *7–8*, 347.
[180] K.-F. Giebel, C. Bechinger, S. Herminghaus, M. Riedel, P. Leiderer, U. Weiland, M. Bastmeyer, *Biophys. J.* **1999**, *76*, 509.
[181] A. Janshoff, K.-P. Dancil, C. Steinem, D. P. Greiner, V. S.-Y. Lin, C. Gurtner, K. Motesharei, M. J. Sailor, M. R. Ghadiri, *J. Am. Chem. Soc.* **1998**, *120*, 12108.
[182] N. Y. Kim, P. E. Laibinis, *J. Am. Chem. Soc* **1998**, *120*, 4516.
[183] J. H. Song, M. J. Sailor, *J. Am. Chem. Soc* **1998**, *120*, 2376.
[184] J. M. Buriak, M. J. Allen, *J. Chem. Am. Soc* **1998**, *120*, 1339.
[185] C. Kößlinger, E. Uttenthaler, S. Drost, F. Aberl, H. Wolf, G. Brink, A. Stanglmaier, E. Sackmann, *Sens. Actuators B* **1995**, *24–25*, 107.
[186] The term cell number includes the detection range under investigation in which a frequency shift was detected.
[187] L. Bao, L. Deng, L. Nie, S. Yao, W. Wei, *Anal. Chim. Acta* **1996**, *319*, 97.
[188] H. Muramatsu, K. T. Kajiwara, E. I. Karube, *Anal. Chim. Acta* **1986**, *188*, 257.
[189] M. Plomer, G. G. Guilbault, B. Hock, *Enzyme Microb. Technol.* **1990**, *14*, 230.
[190] E. Prusak-Sochaczewski, J. H. T. Luong, G. G. Guilbaut, *Enzyme Microb. Technol.* **1990**, *12*, 173.
[191] L. Deng, L. Bao, W. Z. Wei, L. H. Nie, S. Z. Yao, *Enzyme Microb. Technol.* **1996**, *19*, 525.
[192] D. E. Nivens, J. Q. Chambers, T. R. Anderson, D. C. White, *Anal. Chem.* **1993**, *65*, 65.
[193] K. D. Pavey, Z. Ali, C. J. Olliff, F. Paul, *J. Pharm. Biomed. Anal.* **1999**, *20*, 241.
[194] J. Wegener, *Impedanzspektroskopische und mikrogravimetrische Untersuchungen an barrierebildenden Zellen auf planaren Goldelektroden*, PhD thesis, Westfälische Wilhelms-Universität, Münster, **1998**.